

Fast convolution solvers using moment-matching

Xin Liu^a, Qinglin Tang^b, Yong Zhang^{c,d,*}

^a*Eastern Institute for Advanced Study, Eastern Institute of Technology, Ningbo, China, 315200,*

^b*School of Mathematics, Sichuan University, ChengDu, China, 610064,*

^c*Center for Applied Mathematics and KL-AAGDM, Tianjin University, Tianjin, China, 300072,*

^d*State Key Laboratory of Synthetic Biology, Tianjin University, Tianjin, China, 300072.*

Abstract

We propose two easy-to-implement fast algorithms based on moment-matching to compute the nonlocal potential $\varphi(\mathbf{x}) = (U * \rho)(\mathbf{x})$ on bounded domain, where the kernel U is singular at the origin and the density ρ is a fast-decaying smooth function. Each method requires merely minor modifications to commonly-used existing methods, i.e., the sine spectral/Fourier quadrature method, and achieves a much better convergence rate. The key lies in the introduction of a smooth auxiliary function ρ_1 whose moments match those of the density up to an integer order m . Specifically, ρ_1 is constructed using Gaussian function in an explicit way and the associated potential can be calculated analytically. The moments of residual density vanish up to order m , and the corresponding residual potential $U * (\rho - \rho_1)$ decays much faster than the original potential φ at the far field. As for the residual potential evaluation, for classical kernels (e.g., the Coulomb kernel), we solve a differential/pseudo-differential equation on a rectangular domain with homogeneous Dirichlet boundary conditions via sine pseudospectral method, and achieve an arbitrary high convergence rate. While, for general kernels, the regularity of Fourier integrand increase by m thanks to the moments-vanishing property, therefore, the standard trapezoidal rule/midpoint quadrature also converges much faster. To gain a better numerical performance, we utilize the domain expansion technique to obtain better accuracy, and improve the efficiency by simplifying the quadrature into one discrete convolution and applying Fast Fourier Transform (FFT) to a double-sized vector. Rigorous error estimates and extensive numerical investigations showcase the accuracy and efficiency for different nonlocal potentials.

Keywords: convolution integral, moment-matching, domain expansion, tensor acceleration, sine pseudospectral method, error estimates

1. Introduction

In this paper, we focuses on the accurate and efficient evaluation of convolution-type nonlocal potentials

$$\varphi(\mathbf{x}) = (U * \rho)(\mathbf{x}) = \int_{\mathbb{R}^d} U(\mathbf{x} - \mathbf{y})\rho(\mathbf{y})d\mathbf{y}, \quad \mathbf{x} \in \mathbb{R}^d, \quad (1.1)$$

where d is the spatial dimension, the density $\rho(\mathbf{x})$ is a fast-decaying smooth function and the kernel function $U(\mathbf{x})$ is usually singular at the origin. This is a vital and prominent area of research in the science and engineering community.

The convolution (1.1) can be represented equivalently as a Fourier integral

$$\varphi(\mathbf{x}) = \frac{1}{(2\pi)^d} \int_{\mathbb{R}^d} \widehat{U}(\mathbf{k})\widehat{\rho}(\mathbf{k})e^{i\mathbf{k}\cdot\mathbf{x}}d\mathbf{k}, \quad (1.2)$$

*Corresponding author.

Email addresses: xinliu@eitech.edu.cn (Xin Liu), qinglin_tang@scu.edu.cn (Qinglin Tang), Zhang_Yong@tju.edu.cn (Yong Zhang)

where $\widehat{f}(\mathbf{k}) = \int_{\mathbb{R}^d} f(\mathbf{x}) e^{-i\mathbf{k}\cdot\mathbf{x}} d\mathbf{x}$ is the Fourier transform of function $f(\mathbf{x})$. The Fourier transform of density $\widehat{\rho}(\mathbf{k})$ is smooth and decays fast at the far field. The Fourier transform of the kernel $\widehat{U}(\mathbf{k})$ is singular too, and, sometimes, the singularity is too strong such that the above integral is not well-defined for general density. A widely-used approach, named as *Fourier spectral method* (FS) [7] hereafter, discretizes the integral using trapezoidal rule and the resulting quadrature is implemented by Fast Fourier Transform (FFT). Naive ignorance or improper treatment of the singularity shall render severe accuracy lost [7] or reach a saturation, which is also named as “numerical locking phenomenon” in [8].

As far as we know, several efficient and accurate algorithms have been proposed to deal with the singularity, such as the NonUniform Fast Fourier Transform method (NUFFT)-based algorithm [12], Gaussian-Summation method (GauSum) [9, 10], Kernel Truncation Method (KTM) [20, 14, 17], Anisotropic Truncated Kernel Method (ATKM) [11] and the newly-developed far-field smooth approximation (FSA)-based method [15]. All these methods focus on the integral form (1.1) or (1.2), and achieve spectral accuracy while maintaining FFT-like efficiency.

Besides the integral representation, one common way is to solve a partial differential or fractional differential equation, such as the 3D Poisson and 2D Coulomb potential [4, 5, 6], on bounded domain with appropriate boundary conditions. For example, to solve the 3D Poisson equation with sine pseudospectral (SP) method [5], we first truncate the whole space into a bounded rectangular domain $\Omega := [-L, L]^d$ and impose homogeneous Dirichlet boundary conditions. Then we apply sine pseudospectral method and utilize the discrete sine transform to help achieve great efficiency. Unfortunately, the numerical accuracy cease to improve but become saturated instead as the mesh size tends smaller on a fixed computational domain. The saturated accuracy is dominated by errors caused by boundary condition approximation, which is determined by the asymptotics of the potential φ at the far field, and is only first-order with respect to the inverse of domain size in this case.

Despite the “numerical locking”, the SP method gains great popularity in physics community due to its simplicity and implementation easiness. The “locked” accuracy of the numerical solution will become smaller once the boundary condition approximation gets more accurate. In this paper, we introduce an auxiliary function to neutralize the density by moment-matching technique. The associated potential can be computed analytically and the residual potential decays much faster to zero at the far field. Applying SP to solve PDE with homogeneous Dirichlet boundary conditions for the residual potential will alleviate such locking phenomenon or even eliminate it up to a given high precision.

To be specific, if the density satisfies the following vanishing moment conditions

$$\int_{\mathbb{R}^d} \rho(\mathbf{x}) \mathbf{x}^\alpha d\mathbf{x} = 0, \quad |\alpha| = 0, 1, \dots, m, \quad m \in \mathbb{N}, \quad (1.3)$$

where $\alpha = (\alpha_1, \dots, \alpha_d) \in \mathbb{N}^d$ is a multi-index, $\mathbf{x}^\alpha = \prod_{i=1}^d x_i^{\alpha_i}$ and $|\alpha| = \sum_{i=1}^d \alpha_i$, using standard asymptotic analysis, we can prove that the potential decays as fast as

$$|\varphi(\mathbf{x})| \sim \sum_{|\alpha|=m+1} |\partial^\alpha U(\mathbf{x})|, \quad |\mathbf{x}| \rightarrow \infty, \quad (1.4)$$

where $\partial^\alpha U = \partial_{x_1}^{\alpha_1} \cdots \partial_{x_d}^{\alpha_d} U$. Take the 3D Poisson for example, the potential φ decays as fast as $1/|\mathbf{x}|^{m+2}$ at the far field, therefore, the optimal accuracy achieved by SP method is polynomially small as $L^{-(m+2)}$.

Most of the important potentials can be reformulated as PDE or fractional PDE

$$\mathcal{L}\varphi(\mathbf{x}) = \rho(\mathbf{x}), \quad \mathbf{x} \in \mathbb{R}^d, \quad (1.5)$$

where \mathcal{L} is a linear differential operator, for example, $\mathcal{L} = -\Delta$ (2D/3D Poisson) or $\sqrt{-\Delta}$ (2D Coulomb). A more detailed list on linear operators of convolutions is presented in Table 1. For this class of nonlocal potentials, we introduce an auxiliary function $\rho_1(\mathbf{x})$ such that its associated potential $\varphi_1 := U * \rho_1$ can be

computed analytically and its moments match those of the density up to order m , i.e.,

$$\int_{\mathbb{R}^d} \rho_1(\mathbf{x}) \mathbf{x}^\alpha d\mathbf{x} = \int_{\mathbb{R}^d} \rho(\mathbf{x}) \mathbf{x}^\alpha d\mathbf{x}, \quad |\alpha| = 0, 1, \dots, m. \quad (1.6)$$

The residual density $\rho_2 := \rho - \rho_1$ automatically satisfies the vanishing moment conditions (1.3) and its resulting potential $\varphi_2 := U * \rho_2$ is readily solved by SP method.

The construction of auxiliary function turns into the core problem and is of essential importance. So far as we know, there are not so many literature focusing on such topic [3, 8]. In [3], the author proposed compact polynomial mollifiers as the auxiliary function to compute the Poisson potential in the whole space. Such a polynomial-type function is non-smooth, so is the residual density. On the one hand, the convergence rate of SP method, when applied to solve φ_2 , is limited by the regularity of ρ_2 , thus, it requires a small spatial mesh size h to achieve high precision. On the other hand, the discretization of Fourier integral should be carried out on a relatively large domain $[-\pi/h, \pi/h]^d$, because the Fourier integrand $\widehat{U}(\mathbf{k})\widehat{\rho}_2(\mathbf{k})e^{i\mathbf{k}\cdot\mathbf{x}}$ decays only polynomially fast at the far field. Therefore, accurate evaluation of residual potential φ_2 requires a very small mesh size h and shall eventually suffer from a severe efficiency degradation. It is more natural to adopt smooth auxiliary function so to overcome such difficulty. In fact, Bao et al. [8] utilized Gaussian and its first-order derivative to construct a smooth auxiliary function successfully for the 2D Poisson potential. Based on these facts, we propose one auxiliary function as a linear combination of Gaussian and its derivatives up to order m , i.e.,

$$\rho_1(\mathbf{x}) = \sum_{|\alpha|=0}^m \gamma_\alpha \frac{\partial^\alpha G(\mathbf{x})}{\partial \mathbf{x}^\alpha}, \quad \text{with } G(\mathbf{x}) = \frac{1}{(2\pi\sigma^2)^{d/2}} e^{-\frac{|\mathbf{x}|^2}{2\sigma^2}}. \quad (1.7)$$

The coefficients γ_α are determined by the moment-matching conditions (1.6) and are computed analytically by solving a linear system. With the above Gaussian-type auxiliary function, the analytical computation of φ_1 is quite feasible for the common kernels, including Poisson, Coulomb and Biharmonic kernels. While for the general kernels, one may resort to high-order numerical integration, for example, the Gauss-Kronrod quadrature. We skip details here for a more smooth presentation and refer the readers to subsection 2.1.

Apart from the above common potentials, there exists another large class of potentials that can not be written as a PDE or fractional PDE (1.5) but given by Fourier integrals (1.2). As stated before, with a simple computation, we know that the first m -th order Taylor expansion of $\widehat{\rho}_2(\mathbf{k})$ at $\mathbf{k} = 0$ vanish, that is,

$$\left. \frac{\partial^\alpha \widehat{\rho}_2(\mathbf{k})}{\partial \mathbf{k}^\alpha} \right|_{\mathbf{k}=0} = \int_{\mathbb{R}^d} \rho_2(\mathbf{x}) \mathbf{x}^\alpha d\mathbf{x} = 0, \quad (1.8)$$

thus the regularity of Fourier integrand $\widehat{U}(\mathbf{k})\widehat{\rho}_2(\mathbf{k})e^{i\mathbf{k}\cdot\mathbf{x}}$ gets elevated by order m . As a result, the accuracy of quadrature, such as the trapezoidal or midpoint rule, for the Fourier integral is improved to $\mathcal{O}((\Delta k)^p)$, where Δk is the mesh size in Fourier space and the integer p depends on the moment-matching order m and kernel U . Clearly, the numerical accuracy can be improved by increasing the convergence order p or decreasing the mesh size $\Delta k = \pi/L$, equivalently, increasing the domain size L .

In this article, we derive rigorous error analysis for both methods, and prove that the convergence order p increases as m gets larger. For example, for the 3D Poisson potential, the saturated accuracy achieved with SP method scales as $\mathcal{O}(L^{-1})$, while the optimal accuracy with our proposed method is improved to $\mathcal{O}(L^{-(m+2)})$. Most notably, when applied to the 2D Poisson potential, the SP method is *not effective at all* because the potential grows logarithmically fast [16], while, the optimal accuracy achieved with our method is as small as $\mathcal{O}(L^{-(m+1)})$.

For a given integer m , to further improve the accuracy, we adopt the domain expansion [3] and denote the so-called *domain expansion factor* by S . The memory costs and the computational complexity are $\mathcal{O}((SN)^d)$ and $\mathcal{O}((SN)^d \log(SN)^d)$ respectively, where N is the number of grids in each spatial dimension. In a companion paper [2], Anderson proposed a recursive expanding domain method to help reduce the

memory costs down to $\mathcal{O}(S^{d-1}N^d)$ and the complexity, which becomes more favorable with S as

$$\mathcal{O}((S^{d-1}N^d)\log(S^{d-1}N^d)).$$

Clearly, a large S helps improve the accuracy at the sacrifice of efficiency.

Actually, similar to ATKM [11] and FSA [15], both methods proposed here can be simplified to a discrete convolution with tensor explicitly given by Eqn. (2.27) or Eqn. (2.28). Once the tensor is computed out *once for all* in the precomputation step, the essential execution involves merely a pair of FFT/iFFT of a double-sized density. The computational complexity becomes independent of S and is greatly reduced to

$$\mathcal{O}((2N)^d\log(2N)^d).$$

Such tensor acceleration technique greatly improves the efficiency, especially when the potentials are frequently evaluated with the same numerical setup, such as in computing the ground state and dynamics of the nonlocal Schrödinger equation [4, 21].

The paper is organized as follows. In Section 2, we present two simple and high-order fast solvers for nonlocal potential evaluation, along with tensor-based acceleration. Error estimates are provided in Section 3. In Section 4, extensive numerical investigations are conducted to demonstrate the accuracy and efficiency for various kernels. Finally, some conclusions are drawn in Section 5.

2. Fast convolution solvers

In this section, we develop fast convolution solvers using moment-matching technique for the density. The key observation is that the vanishing of the moments of ρ up to order m provides the following advantages:

- (a) The potential generated by ρ decays faster at the far field. (2.9)
- (b) The regularity of integrand in Fourier integral (1.2) gets elevated.

Advantage (a) follows from standard asymptotic analysis of the potential at the far-field, with details provided in Lemma 1 below. This implies that the homogeneous Dirichlet boundary condition approximation becomes more accurate, and it is then very convenient to apply sine pseudospectral method. Advantage (b) follows from Eqn. (1.8), which ensures that the discretization error in evaluating (1.2) decays more rapidly with respect to the mesh size in Fourier space.

Based on the above facts, we introduce an auxiliary function ρ_1 , whose potential can be computed with ease, such that the moments of $\rho_2 = \rho - \rho_1$ vanish up to order m . For clarity, we provide a simple procedure for solving $\varphi = U * \rho$ consisting of the following steps:

Procedure Moment-matching method for potentials $\varphi(\mathbf{x}) = (U * \rho)(\mathbf{x})$.

- 1: Create a auxiliary function $\rho_1(\mathbf{x})$ so that the moments of $\rho_2(\mathbf{x}) = \rho(\mathbf{x}) - \rho_1(\mathbf{x})$ vanish up to order m :

$$\int_{\mathbb{R}^d} \rho_2(\mathbf{x}) \mathbf{x}^\alpha d\mathbf{x} = 0, \quad |\alpha| = 0, 1, \dots, m. \quad (2.10)$$

- 2: Compute $\varphi_1(\mathbf{x}) = (U * \rho_1)(\mathbf{x})$ analytically.
- 3: Compute $\varphi_2(\mathbf{x}) = (U * \rho_2)(\mathbf{x})$ using the SP method or FS method.
- 4: Set $\varphi = \varphi_1 + \varphi_2$.

Lemma 1 (Far-field asymptotic analysis). *For a smooth and numerical compactly supported function $\rho(\mathbf{x})$, the asymptotic behavior of the nonlocal potential at the far field reads as follows*

$$|\varphi(\mathbf{x})| \sim \sum_{|\boldsymbol{\alpha}|=m+1} |\partial^{\boldsymbol{\alpha}} U(\mathbf{x})|, \quad \text{as } |\mathbf{x}| \rightarrow \infty, \quad (2.11)$$

if the moments of $\rho(\mathbf{x})$ vanish up to order m , i.e.,

$$\int_{\mathbb{R}^d} \rho(\mathbf{x}) \mathbf{x}^{\boldsymbol{\alpha}} d\mathbf{x} = 0, \quad |\boldsymbol{\alpha}| = 0, 1, \dots, m. \quad (2.12)$$

Proof. Without loss of generality, we assume that $\text{supp}\{\rho\} \subsetneq \Omega_0$, and define Ω as an expanded domain, i.e., $\Omega_0 \subsetneq \Omega$. Using the Taylor formula with integral remainder for kernel U , we have

$$U(\mathbf{x} - \mathbf{y}) = \sum_{k=0}^m \sum_{|\boldsymbol{\alpha}|=k} \frac{1}{\boldsymbol{\alpha}!} (-1)^{|\boldsymbol{\alpha}|} \partial^{\boldsymbol{\alpha}} U(\mathbf{x}) \mathbf{y}^{\boldsymbol{\alpha}} + r_m, \quad \mathbf{x} \in \partial\Omega, \quad \mathbf{y} \in \Omega_0, \quad (2.13)$$

where $\boldsymbol{\alpha} = (\alpha_1, \alpha_2, \dots, \alpha_d) \in \mathbb{N}^d$ is a multi-index, $|\boldsymbol{\alpha}| = \sum_{i=1}^d \alpha_i$, $\mathbf{y}^{\boldsymbol{\alpha}} = \prod_{i=1}^d y_i^{\alpha_i}$, $\partial^{\boldsymbol{\alpha}} U = \partial_{x_1}^{\alpha_1} \cdots \partial_{x_d}^{\alpha_d} U$, $\boldsymbol{\alpha}! = \alpha_1! \cdots \alpha_d!$ and the integral remainder

$$r_m = (m+1) \sum_{|\boldsymbol{\beta}|=m+1} \frac{1}{\boldsymbol{\beta}!} (-1)^{m+1} \mathbf{y}^{\boldsymbol{\beta}} \int_0^1 \partial^{\boldsymbol{\beta}} U(\mathbf{x} - s\mathbf{y}) (1-s)^m ds.$$

Using Eqn. (2.13) and $\text{supp}\{\rho\} \subsetneq \Omega_0$, for $\mathbf{x} \in \partial\Omega$, we obtain

$$\begin{aligned} \varphi(\mathbf{x}) &= \int_{\mathbb{R}^d} U(\mathbf{x} - \mathbf{y}) \rho(\mathbf{y}) d\mathbf{y} = \int_{\Omega_0} U(\mathbf{x} - \mathbf{y}) \rho(\mathbf{y}) d\mathbf{y} \\ &= \sum_{k=0}^m \sum_{|\boldsymbol{\alpha}|=k} \frac{1}{\boldsymbol{\alpha}!} (-1)^{|\boldsymbol{\alpha}|} \partial^{\boldsymbol{\alpha}} U(\mathbf{x}) \left[\int_{\mathbb{R}^d} \rho(\mathbf{y}) \mathbf{y}^{\boldsymbol{\alpha}} d\mathbf{y} \right] + \int_{\Omega_0} r_m \rho(\mathbf{y}) d\mathbf{y}. \end{aligned}$$

Using the moment conditions (2.12), we have

$$\begin{aligned} |\varphi(\mathbf{x})| &= \left| \int_{\Omega_0} r_m \rho(\mathbf{y}) d\mathbf{y} \right| \lesssim \sum_{|\boldsymbol{\beta}|=m+1} \max_{0 \leq s \leq 1} \left| \int_{\Omega_0} \partial^{\boldsymbol{\beta}} U(\mathbf{x} - s\mathbf{y}) \mathbf{y}^{\boldsymbol{\beta}} \rho(\mathbf{y}) d\mathbf{y} \right| \\ &\lesssim \sum_{|\boldsymbol{\beta}|=m+1} \max_{\substack{\mathbf{y} \in \Omega_0 \\ 0 \leq s \leq 1}} |\partial^{\boldsymbol{\beta}} U(\mathbf{x} - s\mathbf{y})|, \quad \mathbf{x} \in \partial\Omega, \\ &\sim \sum_{|\boldsymbol{\beta}|=m+1} |\partial^{\boldsymbol{\beta}} U(\mathbf{x})|, \quad |\mathbf{x}| \rightarrow \infty. \end{aligned} \quad (2.14)$$

□

2.1. Auxiliary function

To ensure the computational viability of the proposed procedure, we present a specific scheme for constructing the auxiliary function $\rho_1(\mathbf{x})$ and its induced potential $\varphi_1(\mathbf{x})$. There are various ways to construct such a function, such as compact polynomial mollifiers [3]. However, these mollifiers are not smooth and shall eventually lead to severe efficiency degradation. To overcome this issue, we construct the auxiliary function as a linear combination of smooth Gaussian and its derivatives up to order m , as given in (1.7).

The coefficients γ_α are obtained by solving the following linear system

$$\sum_{|\alpha|=0}^m \left[\int_{\mathbb{R}^d} \frac{\partial^\alpha G(\mathbf{x})}{\partial \mathbf{x}^\alpha} \mathbf{x}^\beta d\mathbf{x} \right] \gamma_\alpha = \int_{\mathbb{R}^d} \rho(\mathbf{x}) \mathbf{x}^\beta d\mathbf{x} \quad \text{for } |\beta| = 0, \dots, m. \quad (2.15)$$

In fact, the coefficient matrix $H_\beta^\alpha := \int_{\mathbb{R}^d} \frac{\partial^\alpha G(\mathbf{x})}{\partial \mathbf{x}^\alpha} \mathbf{x}^\beta d\mathbf{x}$ is the lower triangle, therefore the solution to equations (2.15) can be obtained analytically via back substitution. A detailed derivation is given in Appendix A.

With the coefficients γ_α determined, we can evaluate $\varphi_1 = U * \rho_1$ as follows

$$\varphi_1 = U * \rho_1 = U * \left[\sum_{|\alpha|=0}^m \gamma_\alpha \partial^\alpha G \right] = \sum_{|\alpha|=0}^m \gamma_\alpha \partial^\alpha (U * G). \quad (2.16)$$

An explicit analytical expression for $W := U * G$ can be derived for several classes of potentials, including the 2D/3D Poisson, 2D Coulomb, 3D dipole-dipole interaction (DDI) and 2D/3D biharmonic potentials. Details are provided in Appendix B. For general kernels, one may resort to numerical integration to obtain the accurate evaluation of W . Here, we present a numerical scheme to compute the convolution of two radially symmetric functions in 2D, i.e., $U(\mathbf{x}) = U(r)$ and $G(\mathbf{x}) = G(r)$ with $r = |\mathbf{x}|$, then

$$W(\mathbf{x}) = \int_0^\infty U(s) s ds \int_0^{2\pi} G\left(\sqrt{r^2 + s^2 - 2sr \cos \theta}\right) d\theta,$$

which can be calculated by adaptive Gauss-Kronrod quadrature.

In the following, we present two simple numerical methods to compute φ_2 based on the properties (2.9) induced by moment-vanishing. The first method employs the SP method to solve the corresponding differential equation subjected to homogeneous Dirichlet boundary conditions on a bound domain. We refer to this as the **SP-MM** method, with details provided in Subsection 2.2. The second method discretizes the Fourier integral (1.2) using midpoint rule, and the quadrature is efficiently implemented via FFT. This is referred to as the **FS-MM** method, with details provided in Subsection 2.3. Both methods can achieve arbitrary accuracy with high efficiency thanks to discrete sine transform (DST) or FFT, and rigorous error estimates are provided in Section 3.

2.2. SP-MM method

In this subsecction, we introduce the SP method [18] to discretize the following linear PDE

$$\begin{cases} \mathcal{L}\varphi_2(\mathbf{x}) = \rho_2(\mathbf{x}), & \mathbf{x} \in \Omega, \\ \varphi_2(\mathbf{x})|_{\mathbf{x} \in \partial\Omega} = 0, \end{cases} \quad (2.17)$$

where the operator \mathcal{L} contains only even-order derivatives. Without loss of generality, we denote $\Omega = [-L, L]^d := \mathbf{R}_L$ and discrete it by $N \in 2\mathbb{Z}^+$ equally spaced points in each direction. The mesh size is then given by $h = 2L/N$. For simplicity, we only present the detailed scheme for 1D case. Extension to 2D/3D case is quite straightforward. The spatial grid points are given by $x_j = -L + jh$, $j = 1, 2, \dots, N-1$. Denote the space

$$\begin{aligned} X &= \{f(x) \in C^\infty(\Omega), f(x)|_{x \in \partial\Omega} = 0\}, \\ Y_N &= \text{span}\{\sin(\mu_p(x + L)), p = 1, 2, \dots, N-1\}, \end{aligned}$$

with $\mu_p = \pi p/(2L)$. Let $P_N : X \rightarrow Y_N$ be the standard project operator as

$$(P_N f)(x) = \sum_{p=1}^{N-1} \hat{f}_p^s \sin(\mu_p(x + L)), \quad x \in \Omega,$$

where \hat{f}_p^s , the sine transform coefficients, are defined as

$$\hat{f}_p^s = \frac{1}{L} \int_{-L}^L f(x) \sin(\mu_p(x + L)) dx.$$

The above integral is well approximated by applying the trapezoidal rule, which is given explicitly as follows

$$\hat{f}_p^s = \frac{2}{N} \sum_{j=1}^{N-1} f(x_j) \sin\left(\frac{\pi j p}{N}\right). \quad (2.18)$$

Then the sine pseudospectral discretization for (2.17) reads as

$$\varphi_2^N(x_j) = \sum_{p=1}^{N-1} \frac{(\tilde{\rho}_2)_p^s}{\hat{\mathcal{L}}(\mu_p)} \sin\left(\frac{\pi j p}{N}\right), \quad (2.19)$$

where $(\tilde{\rho}_2)_p^s$, the discrete sine transform coefficients, are defined as (2.18), and $\hat{\mathcal{L}}(\mu_p)$ represent the multiplication operator in Fourier space corresponding to the differential operator \mathcal{L} in physical space, which is given by

$$\hat{\mathcal{L}}(\mu_p) = \langle \mathcal{L}e_p(x), e_p(x) \rangle / \langle e_p(x), e_p(x) \rangle,$$

where $e_p(x) := \sin(\mu_p(x + L))$. For example, $\hat{\mathcal{L}}(\mu_p) = (\mu_p)^2$ for the differential operator $\mathcal{L} = -\partial_{xx}$.

Following the same procedure, we present a specific scheme for the two-dimensional problem. Define the physical index and grid points sets as

$$\begin{aligned} \mathcal{I}_N &:= \{(j, k) \in \mathbb{N}^2 \mid 1 \leq j \leq N-1, 1 \leq k \leq N-1\}, \\ \mathcal{T}_x &:= \{(x_j, y_k) := (-L + jh, -L + kh), \quad (j, k) \in \mathcal{I}_N\}. \end{aligned}$$

The corresponding numerical scheme reads as follows

$$\varphi_2^N(x_j, y_k) = \sum_{(p, q) \in \mathcal{I}_N} \frac{(\tilde{\rho}_2)_{pq}^s}{\hat{\mathcal{L}}(\mu_p, \mu_q)} \sin\left(\frac{\pi j p}{N}\right) \sin\left(\frac{\pi k q}{N}\right), \quad (2.20)$$

where

$$(\tilde{\rho}_2)_{pq}^s = \frac{4}{N^2} \sum_{(j, k) \in \mathcal{I}_N} \rho_2(x_j, y_k) \sin\left(\frac{\pi j p}{N}\right) \sin\left(\frac{\pi k q}{N}\right). \quad (2.21)$$

The proposed scheme is easy to implement and can be efficiently executed using DST with $\mathcal{O}(N^d \log(N^d))$ computational complexity. It is applicable to a large class of kernels, and we summarize some common kernels along with their corresponding differential operator \mathcal{L} in Table 1.

2.3. FS-MM method

In this subsection, we introduce FS-MM method to calculate

$$\varphi_2(\mathbf{x}) = \int_{\mathbb{R}^d} U(\mathbf{x} - \mathbf{y}) \rho_2(\mathbf{y}) d\mathbf{y} = \frac{1}{(2\pi)^d} \int_{\mathbb{R}^d} \hat{U}(\mathbf{k}) \hat{\rho}_2(\mathbf{k}) e^{i\mathbf{k} \cdot \mathbf{x}} d\mathbf{k}. \quad (2.22)$$

Since the modified density ρ_2 is smooth and decays exponentially fast, its Fourier transform $\hat{\rho}_2(\mathbf{k})$ is also smooth and decays fast [18]. Therefore, it is reasonable to truncate the whole space \mathbb{R}^d into a large enough bounded domain \mathcal{D} . The main idea of typical Fourier method is to discrete (2.22) using the trapezoidal rule with a dual mesh $\Delta k = \pi/L$ on the truncation domain $\mathcal{D} = [-\pi/h, \pi/h]^d$. Usually, the Fourier transform of

Table 1: The corresponding differential operator and the far-field asymptotics of φ_2 for common kernels.

	$U(r)$	\mathcal{L}	Far-field asymptotics of φ_2
Coulomb	$2D: \frac{1}{2\pi r}$	$\sqrt{-\Delta}$	$r^{-(m+2)}$
Poisson	$2D: \frac{-1}{2\pi} \ln(r)$	$-\Delta$	$r^{-(m+1)}$
	$3D: \frac{1}{4\pi r}$	$-\Delta$	$r^{-(m+2)}$
Biharmonic	$2D: \frac{-r^2}{8\pi} [\ln(r) - 1]$	$-\Delta^2$	$r^{-(m-1)}$
	$3D: \frac{r}{8\pi}$	$-\Delta^2$	r^{-m}
Yukawa	$2D: \frac{1}{2\pi} K_0(\lambda r)$	$-\Delta + \lambda^2$	$e^{-r} r^{-1/2}$
	$3D: \frac{1}{4\pi r} e^{-\lambda r}$	$-\Delta + \lambda^2$	$e^{-r} r^{-1}$

kernel $\widehat{U}(\mathbf{k})$ is singular at the origin. To avoid the origin, we adopt the midpoint rule instead of trapezoidal rule, and the resulting quadrature still can be efficiently accelerated using FFT within $\mathcal{O}(N^d \log(N^d))$ complexity. Specifically, takeing 2D case as an example, we define the physical index and grid points sets as follows

$$\begin{aligned} \mathcal{J}_N &:= \{(j, k) \in \mathbb{N}^2 \mid -N/2 \leq j \leq N/2 - 1, -N/2 \leq k \leq N/2 - 1\}, \\ \mathcal{G}_{\mathbf{x}} &:= \{(x_j, y_k) := (jh, kh), \quad (j, k) \in \mathcal{J}_N\}. \end{aligned}$$

By discretizing (2.22) using the midpoint rule with a dual mesh $\Delta k = \pi/L$ on the truncation domain $\mathcal{D} = [-\pi/h, \pi/h]^d$, we obtain

$$\varphi_2^N(\mathbf{x}_{jk}) = \frac{1}{(2L)^2} \sum_{(p,q) \in \mathcal{J}_N} \widehat{U}(\nu_{p+\frac{1}{2}}, \nu_{q+\frac{1}{2}}) \widehat{\rho}_2(\nu_{p+\frac{1}{2}}, \nu_{q+\frac{1}{2}}) e^{\frac{2\pi i}{N} [(p+\frac{1}{2})j + (q+\frac{1}{2})k]}, \quad (2.23)$$

where $\mathbf{x}_{jk} := (x_j, y_k)$, $\nu_p = (2\pi p)/(2L)$ and $\nu_q = (2\pi q)/(2L)$. The Fourier transform $\widehat{\rho}_2(\nu_p, \nu_q)$ is well approximated by applying the trapezoidal rule, and the resulting summation is given as follows

$$\widetilde{\rho}_2(\nu_p, \nu_q) = h^2 \sum_{(j,k) \in \mathcal{J}_N} \rho(x_j, y_k) e^{-\frac{2\pi i}{N} (pj + qk)}. \quad (2.24)$$

2.4. Domain expansion and tensor structure simplification

Both the SP-MM and FS-MM methods are simple, efficient and can achieve the arbitrary high order with respect to L^{-1} (see Theorem 1-3). Therefore, the accuracy can be furthermore improved by expanding the computational domain. Without loss of generality, let the expanded domain be $\mathbf{R}_{SL} := [-SL, SL]^d$, where S is referred to as the **domain expansion factor**. Taking FS-MM method as an example, the scheme

(2.23) becomes

$$\varphi_2^N(\mathbf{x}_{jk}) = \frac{1}{(2SL)^2} \sum_{(p,q) \in \mathcal{J}_{SN}} \widehat{U}(\nu_{p+\frac{1}{2}}, \nu_{q+\frac{1}{2}}) \tilde{\rho}_2(\nu_{p+\frac{1}{2}}, \nu_{q+\frac{1}{2}}) e^{\frac{2\pi i}{SN} [(p+\frac{1}{2})j + (q+\frac{1}{2})k]}. \quad (2.25)$$

It is obvious that the accuracy can be improved by choosing a large S , but this bottlenecks the efficiency and puts a heavy burden on memory requirement. Specifically, the memory costs and the computational complexity are $\mathcal{O}((SN)^d)$ and $\mathcal{O}((SN)^d \log(SN)^d)$ respectively. In a companion paper [2], Anderson proposed a recursive expanding domain method to help reduce the memory costs to $\mathcal{O}(S^{d-1}N^d)$ and the complexity to $\mathcal{O}((S^{d-1}N^d) \log(S^{d-1}N^d))$, which becomes more favorable with S . Thus, while a larger S improves accuracy, it inevitably imposes a trade-off in terms of efficiency.

Fortunately, the resulting summation (2.25) can be equivalently reformulated as a discrete convolution structure by plugging (2.24) into (2.25) and switching the summation order, that is,

$$\varphi_2^N(x_j, y_k) = \sum_{(j', k') \in \mathcal{J}_N} T_{j-j', k-k'} (\rho_2)_{j', k'}. \quad (2.26)$$

The tensor T reads explicitly as

$$T_{j,k} = \frac{1}{(SN)^2} \sum_{(p,q) \in \mathcal{J}_{SN}} \widehat{U}(\nu_{p+\frac{1}{2}}, \nu_{q+\frac{1}{2}}) e^{\frac{2\pi i}{SN} [(p+\frac{1}{2})j + (q+\frac{1}{2})k]}, \quad (2.27)$$

and it can be computed out *once for all* within $\mathcal{O}((SN)^2 \log((SN)^2))$ float operations using iFFT.

Once the tensor is available in the precomputation step, the effective computation is merely a pair of FFT and iFFT on a **double-sized** vector [14]. The computational complexity becomes independent of S and is greatly reduced to

$$\mathcal{O}((2N)^d \log(2N)^d).$$

Such tensor acceleration technique greatly improves the efficiency, particularly in scenarios where the potential is frequently evaluated under the same numerical setup, such as in computing the ground state and dynamics of the nonlocal Schrödinger equation [4, 13]. We refer to it as the **FS-Tensor** method.

For SP-MM method, using the identity $\sin(x) = (e^{ix} - e^{-ix})/(2i)$ and the even-odd decomposition (3.43) of density, as described in the proof of Theorem 2, it can equivalently be rewritten as 2^d discrete convolution summations. To be specific, for two-dimensional problem, we obtain

$$\begin{aligned} \varphi_2^N(x_j, y_k) &= \sum_{(j', k') \in \mathcal{J}_N} \left[T_{j-j', k-k'}^{ee} (\rho_2^{ee})_{j', k'} + T_{j-j', k-k'}^{eo} (\rho_2^{eo})_{j', k'} + \right. \\ &\quad \left. T_{j-j', k-k'}^{oe} (\rho_2^{oe})_{j', k'} + T_{j-j', k-k'}^{oo} (\rho_2^{oo})_{j', k'} \right] \\ &:= T^{ee} * \rho_2^{ee} + T^{eo} * \rho_2^{eo} + T^{oe} * \rho_2^{oe} + T^{oo} * \rho_2^{oo}, \end{aligned}$$

where the tensors are given by

$$T_{j,k}^{ee} = \frac{1}{(SN)^2} \sum_{(p,q) \in \mathcal{J}_{SN}} \left(\widehat{\mathcal{L}}(\mu_{2p+1}, \mu_{2q+1}) \right)^{-1} e^{\frac{2\pi i}{SN} [(p+\frac{1}{2})j + (q+\frac{1}{2})k]}, \quad (2.28)$$

$$T_{j,k}^{eo} = \frac{1}{(SN)^2} \sum_{\substack{(p,q) \in \mathcal{J}_{SN} \\ q \neq 0}} \left(\widehat{\mathcal{L}}(\mu_{2p+1}, \mu_{2q}) \right)^{-1} e^{\frac{2\pi i}{SN} [(p+\frac{1}{2})j + qk]}, \quad (2.29)$$

$$T_{j,k}^{oe} = \frac{1}{(SN)^2} \sum_{\substack{(p,q) \in \mathcal{J}_{SN} \\ p \neq 0}} \left(\widehat{\mathcal{L}}(\mu_{2p}, \mu_{2q+1}) \right)^{-1} e^{\frac{2\pi i}{SN} [pj + (q + \frac{1}{2})k]}, \quad (2.30)$$

$$T_{j,k}^{oo} = \frac{1}{(SN)^2} \sum_{(p,q) \in \mathcal{J}_{SN} \setminus \{(0,0)\}} \left(\widehat{\mathcal{L}}(\mu_{2p}, \mu_{2q}) \right)^{-1} e^{\frac{2\pi i}{SN} [pj + qk]}. \quad (2.31)$$

Based on the relation between midpoint rule and rectangle rule given in Theorem 3, the following approximation is valid by neglecting error terms of the same order and above, that is,

$$\begin{aligned} \varphi_2^N &= T^{ee} * \rho_2 + [T^{eo} - T^{ee}] * \rho_2^{eo} + [T^{oe} - T^{ee}] * \rho_2^{oe} + [T^{oo} - T^{ee}] * \rho_2^{oo} \\ &\approx T^{ee} * \rho_2. \end{aligned}$$

Therefore, we can simplify the SP-MM method to a single discrete convolution summation (2.26) with the tensor $T_{j,k} = T_{j,k}^{ee}$. We refer to it as the **SP-Tensor** method. For clarity, we present a detailed step-by-step algorithm proposed in Algorithm 1 using the 2D case.

Algorithm 1 FS-Tensor/SP-Tensor method for $\varphi(\mathbf{x}) = (U * \rho)(\mathbf{x})$.

Input: (i). Precompute $W(\mathbf{x}) := [U * G](\mathbf{x})$ with $G(\mathbf{x}) = \frac{1}{(2\pi\sigma^2)^{d/2}} e^{-\frac{|\mathbf{x}|^2}{2\sigma^2}}$.
(ii). Choose a $m \in \mathbb{N}$ and precompute $\frac{\partial^\alpha G(\mathbf{x})}{\partial \mathbf{x}^\alpha}$, $\frac{\partial^\alpha W(\mathbf{x})}{\partial \mathbf{x}^\alpha}$ with $|\alpha| = 0, \dots, m$.
(iii). Choose a $S \in \mathbb{N}$ and precompute the tensor T by Eqn.(2.27) (FS) or Eqn.(2.28) (SP) via iFFT.

- 1: Compute the coefficients γ_α with $|\alpha| = 0, \dots, m$ (see Appendix A).
- 2: Compute $\rho_1(\mathbf{x}) = \sum_{|\alpha|=0}^m \gamma_\alpha \frac{\partial^\alpha G(\mathbf{x})}{\partial \mathbf{x}^\alpha}$ and $\varphi_1(\mathbf{x}) = \sum_{|\alpha|=0}^m \gamma_\alpha \frac{\partial^\alpha W(\mathbf{x})}{\partial \mathbf{x}^\alpha}$ exactly.
- 3: Set $\rho_2 = \rho - \rho_1$ and compute φ_2 by Eqn.(2.26) via FFT/iFFT.
- 4: Compute $\varphi = \varphi_1 + \varphi_2$.

3. Error estimates

In this section, we provide rigorous error estimates. For the SP-MM method, the SP method achieves spectral accuracy for solving linear differential equations subject to homogeneous Dirichlet boundary conditions. The boundary condition approximation error will dominate as the numerical discretization gets finer because the nonlocal potential does not satisfy homogeneous Dirichlet boundary condition exactly but with an approximation error of some polynomial order in terms of domain size. Detailed error analysis are provided in Theorem 1 and Theorem 2. For the FS-MM method, the error mainly comes from the discretization of Fourier integral using the midpoint rule. Rigorous error analysis are provided in Theorem 3.

To quantify the error estimates, we define the following norm

$$\|\varphi - \tilde{\varphi}\|_{\infty(\Omega)} := \sup_{\mathbf{x} \in \Omega} |(\varphi - \tilde{\varphi})(\mathbf{x})|,$$

and we use $A \lesssim B$ to denote $A \leq cB$ where $c > 0$ is a constant. For simplification of notations, below we omit the 2 in the symbols of ρ_2 and φ_2 .

For the SP-MM method, we aim to derive the error $\|\varphi - \tilde{\varphi}\|_{\infty(\Omega)}$, where $\varphi = U * \rho$ and $\tilde{\varphi}$ satisfies

the differential equation

$$\begin{cases} \mathcal{L}\tilde{\varphi}(\mathbf{x}) = \rho(\mathbf{x}), & \mathbf{x} \in \Omega, \\ \tilde{\varphi}(\mathbf{x})|_{\mathbf{x} \in \partial\Omega} = 0. \end{cases} \quad (3.32)$$

If the maximum norm estimate holds for the equation (3.32), we have the following theorem.

Theorem 1 (SP-MM method). *For a smooth and compactly supported function $\rho(\mathbf{x})$ that satisfies the vanishing moment condition (1.3), the following estimate*

$$\|\varphi - \tilde{\varphi}\|_{\infty(\Omega)} \lesssim \sum_{|\beta|=m+1} \max_{\substack{\mathbf{x} \in \partial\Omega \\ \mathbf{y} \in \Omega_0 \\ 0 \leq s \leq 1}} |\partial^\beta U(\mathbf{x} - s\mathbf{y})|$$

holds true, where $\Omega_0 := \text{supp}\{\rho\} \subset \Omega$.

Proof. Let $w = \varphi - \tilde{\varphi}$, using $\mathcal{L}\varphi = \rho$ with $\mathbf{x} \in \mathbb{R}^d$ and equation (3.32), we obtain

$$\begin{cases} \mathcal{L}w(\mathbf{x}) = 0, & \mathbf{x} \in \Omega, \\ w(\mathbf{x})|_{\mathbf{x} \in \partial\Omega} = \varphi(\mathbf{x})|_{\mathbf{x} \in \partial\Omega}. \end{cases}$$

Using maximum norm estimate [19], we have

$$\|w\|_{\infty(\Omega)} \leq \|w\|_{\infty(\partial\Omega)} = \|\varphi\|_{\infty(\partial\Omega)}.$$

With the help of Lemma 1, taking supremum with respect to \mathbf{x} for inequation (2.14), we obtain

$$\|\varphi - \tilde{\varphi}\|_{\infty(\Omega)} \leq \|\varphi\|_{\infty(\partial\Omega)} \lesssim \sum_{|\beta|=m+1} \max_{\substack{\mathbf{x} \in \partial\Omega \\ \mathbf{y} \in \Omega_0 \\ 0 \leq s \leq 1}} |\partial^\beta U(\mathbf{x} - s\mathbf{y})|.$$

Then the proof is completed. \square

Remark 3.1. For 3D Poisson potential with $U(\mathbf{x}) = \frac{1}{4\pi|\mathbf{x}|}$, we have

$$\|\varphi - \tilde{\varphi}\|_{\infty(\Omega)} \lesssim \sum_{|\beta|=m+1} \max_{\substack{\mathbf{x} \in \partial\Omega \\ \mathbf{y} \in \Omega_0 \\ 0 \leq s \leq 1}} \frac{1}{|\mathbf{x} - s\mathbf{y}|^{m+2}} \lesssim \frac{1}{(L - L_0)^{m+2}},$$

where $\Omega_0 = [-L_0, L_0]^3$ and $\Omega = [-L, L]^3$.

If the maximum norm estimate is not well-established, such as the 2D Coulomb potential, we derive the error estimates from a different perspective. For ease of explanation, we take the 2D Coulomb potential as an example, and error estimates for other potentials can be derived using the same technique. The numerical scheme is given by

$$\varphi_N(x, y) = \sum_{p=1}^{N-1} \sum_{q=1}^{N-1} \frac{\hat{\rho}_{pq}^s}{\sqrt{\mu_p^2 + \mu_q^2}} \sin(\mu_p(x + L)) \sin(\mu_q(y + L)),$$

where

$$\hat{\rho}_{pq}^s = \frac{1}{L^2} \int_{\mathbf{R}_L} \rho(x, y) \sin(\mu_p(x + L)) \sin(\mu_q(y + L)) dx dy.$$

Theorem 2 (SP-MM method for 2D Coulomb potential). *For a smooth and compactly supported function $\rho(\mathbf{x})$ that satisfies the vanishing moment condition (1.3), the following estimate*

$$\|\varphi - \varphi_N\|_{\infty(\Omega)} \lesssim L^{-(m+2)}$$

holds true for 2D Coulomb potential.

Proof. Let $w := \varphi - \varphi_N$, we obtain

$$\begin{cases} -\Delta w(\mathbf{x}) = (-\Delta \varphi(\mathbf{x})) - (-\Delta \varphi_N(\mathbf{x})) := g(\mathbf{x}), & \mathbf{x} \in \mathbf{R}_L, \\ w(\mathbf{x})|_{\mathbf{x} \in \partial \mathbf{R}_L} = \varphi(\mathbf{x})|_{\mathbf{x} \in \partial \mathbf{R}_L}. \end{cases} \quad (3.33)$$

Using the maximum norm estimate, we have

$$\|w\|_{\infty(\mathbf{R}_L)} \leq \|\varphi\|_{\infty(\partial \mathbf{R}_L)} + \|g\|_{\infty(\mathbf{R}_L)}. \quad (3.34)$$

With the help of the Lemma 1, we have

$$\|\varphi\|_{\infty(\partial \mathbf{R}_L)} \lesssim L^{-(m+2)}. \quad (3.35)$$

Next, we focus on estimating $\|g\|_{\infty(\mathbf{R}_L)}$. In fact, $g(\mathbf{x})$ can be equivalently rewritten as

$$\begin{aligned} g(x, y) = & \frac{1}{(2\pi)^2} \int_{\mathbb{R}^2} \sqrt{k_1^2 + k_2^2} \hat{\rho}(k_1, k_2) e^{i(k_1 x + k_2 y)} dk_1 dk_2 - \\ & \sum_{p=1}^{N-1} \sum_{q=1}^{N-1} \sqrt{\mu_p^2 + \mu_q^2} \hat{\rho}_{pq}^s \sin(\mu_p(x + L)) \sin(\mu_q(y + L)). \end{aligned} \quad (3.36)$$

Our idea is to utilize the relationship

$$\sin(x) = (e^{ix} - e^{-ix})/(2i) \quad (3.37)$$

to transform $\sin(x)$ function in (3.36) into e^{ix} function. Specifically, a tedious computation shows that

$$\begin{aligned} -\Delta \varphi_N &= \sum_{p=1}^{N-1} \sum_{q=1}^{N-1} \sqrt{\mu_p^2 + \mu_q^2} \hat{\rho}_{pq}^s \left(\frac{e^{i\mu_p(x+L)} - e^{-i\mu_p(x+L)}}{2i} \right) \left(\frac{e^{i\mu_q(y+L)} - e^{-i\mu_q(y+L)}}{2i} \right) \\ &= -\frac{1}{4} \sum_{p=1}^{N-1} \sum_{q=1}^{N-1} \sqrt{\mu_p^2 + \mu_q^2} \hat{\rho}_{pq}^s \left(e^{i[\mu_p(x+L) + \mu_q(y+L)]} - e^{i[\mu_p(x+L) - \mu_q(y+L)]} \right. \\ &\quad \left. - e^{i[-\mu_p(x+L) + \mu_q(y+L)]} + e^{-i[\mu_p(x+L) + \mu_q(y+L)]} \right). \end{aligned}$$

Noted that $\hat{\rho}_{p(-q)}^s = -\hat{\rho}_{pq}^s$, we have

$$\begin{aligned} & \sum_{p=1}^{N-1} \sum_{q=1}^{N-1} \sqrt{\mu_p^2 + \mu_q^2} \hat{\rho}_{pq}^s e^{i[\mu_p(x+L) - \mu_q(y+L)]} \\ = & \sum_{p=1}^{N-1} \sum_{q=-N+1}^{-1} \sqrt{\mu_p^2 + \mu_q^2} (-\hat{\rho}_{pq}^s) e^{i[\mu_p(x+L) + \mu_q(y+L)]} \end{aligned}$$

In a similar way, we have

$$-\Delta\varphi_N = -\frac{1}{4} \sum_{\substack{p=-N+1 \\ p \neq 0}}^{N-1} \sum_{\substack{q=-N+1 \\ q \neq 0}}^{N-1} \sqrt{\mu_p^2 + \mu_q^2} \hat{\rho}_{pq}^s e^{i(\mu_p + \mu_q)L} e^{i(\mu_p x + \mu_q y)}. \quad (3.38)$$

Next, we aim to derive the relationship between $\hat{\rho}^s$ and $\hat{\rho}$. Using Eqn. (3.37), we have

$$\begin{aligned} \hat{\rho}_{pq}^s = & -\frac{1}{4L^2} \int_{\mathbf{R}_L} \rho(x, y) \left(e^{i[\mu_p(x+L) + \mu_q(y+L)]} - e^{i[\mu_p(x+L) - \mu_q(y+L)]} \right. \\ & \left. - e^{i[-\mu_p(x+L) + \mu_q(y+L)]} + e^{-i[\mu_p(x+L) + \mu_q(y+L)]} \right) dx dy. \end{aligned}$$

For the first term, we apply the change of variables $x \mapsto -x$ and $y \mapsto -y$ in the integral to obtain

$$\begin{aligned} & \int_{\mathbf{R}_L} \rho(x, y) e^{i[\mu_p(x+L) + \mu_q(y+L)]} dx dy \\ = & \int_{\mathbf{R}_L} \rho(-x, -y) e^{i[\mu_p(-x+L) + \mu_q(-y+L)]} dx dy \\ = & \int_{\mathbf{R}_L} (-1)^{p+q} \rho(-x, -y) e^{-i[\mu_p(x+L) + \mu_q(y+L)]} dx dy. \end{aligned}$$

Therefore, we obtain

$$\begin{aligned} \hat{\rho}_{pq}^s = & -\frac{1}{4L^2} \int_{\mathbf{R}_L} \left[(-1)^{p+q} \rho(-x, -y) - (-1)^p \rho(-x, y) - (-1)^q \rho(x, -y) + \rho(x, y) \right] \\ & e^{-i[\mu_p(x+L) + \mu_q(y+L)]} dx dy. \end{aligned}$$

If the density ρ is an odd or even function, the above expression can be further simplified. However, the density ρ does not generally exhibit such parity properties. Fortunately, any univariate function can be decomposed into the sum of an even and an odd function. Thus, we prove the result separately for the following four cases.

Case 1: When $\rho(x, y)$ is even with respect to both x and y , i.e., $\rho(-x, y) = \rho(x, y)$ and $\rho(x, -y) = \rho(x, y)$, we have

$$\begin{aligned} \hat{\rho}_{pq}^s = & -\frac{1}{4L^2} e^{-i(\mu_p + \mu_q)L} [1 - (-1)^p] [1 - (-1)^q] \int_{\mathbf{R}_L} \rho(x, y) e^{-i(\mu_p x + \mu_q y)} dx dy \\ = & \begin{cases} -\frac{1}{L^2} e^{-i(\mu_p + \mu_q)L} \hat{\rho}(\mu_p, \mu_q), & p \text{ odd \& } q \text{ odd,} \\ 0, & \text{else.} \end{cases} \end{aligned} \quad (3.39)$$

Plugging (3.39) into (3.38), $-\Delta\varphi_N$ can be simplified as

$$\begin{aligned}
-\Delta\varphi_N &= \frac{1}{4L^2} \sum_{p=-N/2}^{N/2-1} \sum_{q=-N/2}^{N/2-1} \sqrt{\mu_{2p+1}^2 + \mu_{2q+1}^2} \widehat{\rho}(\mu_{2p+1}, \mu_{2q+1}) e^{i(\mu_{2p+1}x + \mu_{2q+1}y)} \\
&= \frac{1}{4L^2} \sum_{p=-N/2}^{N/2-1} \sum_{q=-N/2}^{N/2-1} \sqrt{\nu_{p+\frac{1}{2}}^2 + \nu_{q+\frac{1}{2}}^2} \widehat{\rho}(\nu_{p+\frac{1}{2}}, \nu_{q+\frac{1}{2}}) e^{i(\nu_{p+\frac{1}{2}}x + \nu_{q+\frac{1}{2}}y)}, \\
&:= \left(\frac{2\pi}{2L}\right)^2 \sum_{p=-N/2}^{N/2-1} \sum_{q=-N/2}^{N/2-1} f(\nu_{p+\frac{1}{2}}, \nu_{q+\frac{1}{2}}),
\end{aligned}$$

where $f(k_1, k_2) := \frac{1}{(2\pi)^2} \sqrt{k_1^2 + k_2^2} \widehat{\rho}(k_1, k_2) e^{i(k_1x + k_2y)}$, $\nu_p = (2\pi p)/(2L)$ and $\nu_q = (2\pi q)/(2L)$. Note that f depends on x and y . For simplicity, we omit the explicit dependence on x and y in the notation. Since $\widehat{\rho}$ is compactly supported, f is also compactly supported. Therefore, it is reasonable to choose a fixed mesh size h such that $\text{supp}\{\widehat{f}\} \subsetneq R_h := [-\pi/h, \pi/h]^2$. In this case, the function g in (3.36) equivalently becomes

$$\begin{aligned}
g &= \int_{R_h} f(k_1, k_2) dk_1 dk_2 - \left(\frac{2\pi}{2L}\right)^2 \sum_{p=-N/2}^{N/2-1} \sum_{q=-N/2}^{N/2-1} f(\nu_{p+\frac{1}{2}}, \nu_{q+\frac{1}{2}}) \\
&:= \int_{R_h} f(k_1, k_2) dk_1 dk_2 - Q^{\text{MM}}(f) := E^{\text{MM}}(f).
\end{aligned}$$

Clearly, g is the discretization error of the midpoint rule. We consider the Fourier series expansion of f and denote

$$P_K(f)(k_1, k_2) := \sum_{p=-K}^K \sum_{q=-K}^K \widehat{f}_{pq} e^{i(\lambda_p k_1 + \lambda_q k_2)},$$

where $\lambda_p = \frac{2\pi}{2\pi/h} p = ph$ and the Fourier coefficients are given as follows

$$\begin{aligned}
\widehat{f}_{pq} &= \frac{1}{|R_h|} \int_{R_h} f(k_1, k_2) e^{-i(\lambda_p k_1 + \lambda_q k_2)} dk_1 dk_2 \\
&= \frac{1}{|R_h|} \frac{1}{(2\pi)^2} \int_{R_h} \sqrt{k_1^2 + k_2^2} \widehat{\rho}(k_1, k_2) e^{i[k_1(x-\lambda_p) + k_2(y-\lambda_q)]} dk_1 dk_2 \\
&= -\frac{h^2}{4\pi^2} \Delta\varphi(x - \lambda_p, y - \lambda_q).
\end{aligned}$$

For simplicity, we define $\mathbf{p} = (p, q)$ and $\mathcal{T}_K := \{(p, q) \in \mathbb{Z}^2, p = -K, \dots, K, q = -K, \dots, K\}$. By leveraging continuity and piecewise differentiability of f , along with the following estimates

$$\begin{aligned}
\left| \sum_{(p,q) \notin \mathcal{T}_K} \widehat{f}_{pq} e^{i(\lambda_p k_1 + \lambda_q k_2)} \right| &\leq \sum_{(p,q) \notin \mathcal{T}_K} \left| \widehat{f}_{pq} \right| \lesssim \sum_{|\mathbf{p}| > K} \left| \widehat{f}_{\mathbf{p}} \right| \\
&\lesssim \sum_{|\mathbf{p}| > K} |\Delta\varphi(\mathbf{x} - \mathbf{p}h)| \lesssim \sum_{|\mathbf{p}| > K} \frac{1}{|\mathbf{p}h - \mathbf{x}|^{(m+4)}} \lesssim \sum_{|\mathbf{p}| > K} \frac{1}{|\mathbf{p} - \frac{\mathbf{x}}{h}|^{m+4}} \\
&\lesssim \int_K^\infty \frac{1}{|\mathbf{x}| - \frac{\sqrt{2}L}{h}|^{m+4}} d\mathbf{x} = 2\pi \int_K^\infty \frac{r}{|r - \frac{\sqrt{2}L}{h}|^{m+4}} dr \\
&\lesssim \frac{1}{K^{m+2}} \rightarrow 0, \quad K \rightarrow +\infty,
\end{aligned}$$

we obtain that f has a uniformly convergent Fourier series, i.e.,

$$f = \sum_{p=-\infty}^{\infty} \sum_{q=-\infty}^{\infty} \hat{f}_{pq} e^{i(\lambda_p k_1 + \lambda_q k_2)}.$$

Using the linearity of $E^{\text{MM}}(f)$ and the uniform convergence of the Fourier series of f , we have

$$E^{\text{MM}}(f) = \sum_{p=-\infty}^{\infty} \sum_{q=-\infty}^{\infty} \hat{f}_{pq} E^{\text{MM}}\left(e^{i(\lambda_p k_1 + \lambda_q k_2)}\right). \quad (3.40)$$

A simple calculation shows that

$$E^{\text{MM}}\left(e^{i(\lambda_p k_1 + \lambda_q k_2)}\right) = \begin{cases} -\left(\frac{2\pi}{h}\right)^2 (-1)^{p+q}, & p, q \in N\mathbb{N}^+, \\ 0, & \text{else.} \end{cases} \quad (3.41)$$

By plugging Eqn. (3.41) into Eqn. (3.40) and using Lemma 1, we have

$$\begin{aligned} |g| &= |E^{\text{MM}}(f)| = \left| -\left(\frac{2\pi}{h}\right)^2 \sum_{|p|>0} \sum_{|q|>0} (-1)^{(p+q)N} \hat{f}_{pN,qN} \right| \\ &\lesssim \sum_{|p|>0} \sum_{|q|>0} \left| \Delta\varphi(x - \lambda_{pN}, y - \lambda_{qN}) \right| \lesssim \sum_{|\mathbf{p}|>0} \frac{1}{|\mathbf{x} - 2L\mathbf{p}|^{m+4}} \\ &= \frac{1}{L^{m+4}} \sum_{|\mathbf{p}|>0} \frac{1}{|\mathbf{p} - \frac{\mathbf{x}}{2L}|^{m+4}} \lesssim \frac{1}{L^{m+4}}. \end{aligned}$$

Case 2: When $\rho(x, y)$ is even with respect to x and odd with respect to y , i.e., $\rho(-x, y) = \rho(x, y)$ and $\rho(x, -y) = -\rho(x, y)$, we have

$$\begin{aligned} \hat{\rho}_{pq}^s &= -\frac{1}{4L^2} e^{-i(\mu_p + \mu_q)L} [1 - (-1)^p] [1 + (-1)^q] \int_{\mathbf{R}_L} \rho(x, y) e^{-i(\mu_p x + \mu_q y)} dx dy \\ &= \begin{cases} -\frac{1}{L^2} e^{-i(\mu_p + \mu_q)L} \hat{\rho}(\mu_p, \mu_q), & p \text{ odd \& } q \text{ even,} \\ 0, & \text{else.} \end{cases} \end{aligned} \quad (3.42)$$

Similarly, by plugging (3.42) into (3.38), $-\Delta\varphi_N$ can be further simplified as

$$-\Delta\varphi_N = \left(\frac{2\pi}{2L}\right)^2 \sum_{p=-N/2}^{N/2-1} \sum_{\substack{q=-N/2+1 \\ q \neq 0}}^{N/2-1} f(\nu_{p+\frac{1}{2}}, \nu_q) = \left(\frac{2\pi}{2L}\right)^2 \sum_{p=-N/2}^{N/2-1} \sum_{q=-N/2}^{N/2-1} f(\nu_{p+\frac{1}{2}}, \nu_q),$$

where the second equality holds because $f(\nu_{p+\frac{1}{2}}, \nu_0) = f(\nu_{p+\frac{1}{2}}, \nu_{-N/2}) = 0$. Then the function g in (3.36) equivalently becomes

$$\begin{aligned} g &= \int_{R_h} f(k_1, k_2) dk_1 dk_2 - \left(\frac{2\pi}{2L}\right)^2 \sum_{p=-N/2}^{N/2-1} \sum_{q=-N/2}^{N/2-1} f(\nu_{p+\frac{1}{2}}, \nu_q) \\ &:= \int_{R_h} f(k_1, k_2) dk_1 dk_2 - Q^{\text{ML}}(f) = E^{\text{ML}}(f). \end{aligned}$$

Similar to Case 1, we have

$$\begin{aligned}
|g| &= |E^{\text{ML}}(f)| = \left| \sum_{p=-\infty}^{\infty} \sum_{q=-\infty}^{\infty} \hat{f}_{pq} E^{\text{ML}}(e^{i(\lambda_p k_1 + \lambda_q k_2)}) \right| \\
&= \left| -\left(\frac{2\pi}{h}\right)^2 \sum_{|p|>0} \sum_{|q|>0} (-1)^{pN} \hat{f}_{pN,qN} \right| \lesssim \sum_{|p|>0} \sum_{|q|>0} |\Delta\varphi(x - \lambda_{pN}, y - \lambda_{qN})| \\
&\lesssim \sum_{|\mathbf{p}|>0} \frac{1}{|\mathbf{x} - 2L\mathbf{p}|^{m+4}} \lesssim \frac{1}{L^{m+4}}.
\end{aligned}$$

Case 3: When $\rho(x, y)$ is odd with respect to x and even with respect to y , i.e., $\rho(-x, y) = -\rho(x, y)$ and $\rho(x, -y) = \rho(x, y)$, the proof is analogous to Case 1 and Case 2. For brevity, the detailed steps are omitted.

Case 4: When $\rho(x, y)$ is odd with respect to both x and y , i.e., $\rho(-x, y) = -\rho(x, y)$ and $\rho(x, -y) = -\rho(x, y)$, the proof is analogous to Case 1 and Case 2. For brevity, the detailed steps are omitted.

For general density ρ , we perform an odd-even decomposition, i.e.,

$$\rho(x, y) = \rho^{ee}(x, y) + \rho^{eo}(x, y) + \rho^{oe}(x, y) + \rho^{oo}(x, y), \quad (3.43)$$

where

$$\begin{aligned}
\rho^{ee}(x, y) &= \frac{1}{4} [\rho(x, y) + \rho(x, -y) + \rho(-x, y) + \rho(-x, -y)], \\
\rho^{eo}(x, y) &= \frac{1}{4} [\rho(x, y) - \rho(x, -y) + \rho(-x, y) - \rho(-x, -y)], \\
\rho^{oe}(x, y) &= \frac{1}{4} [\rho(x, y) + \rho(x, -y) - \rho(-x, y) - \rho(-x, -y)], \\
\rho^{oo}(x, y) &= \frac{1}{4} [\rho(x, y) - \rho(x, -y) - \rho(-x, y) + \rho(-x, -y)].
\end{aligned}$$

Importantly, the function $\rho^{\alpha\beta}$ with $\alpha, \beta \in \{e, o\}$ retains the properties of smoothness, compact support and moment-matching (1.3), as dose density ρ . Based on the discussion in Case 1 - Case 4, we have

$$\begin{aligned}
|g| &= |E^{\text{MM}}(f^{ee}) + E^{\text{ML}}(f^{eo}) + E^{\text{LM}}(f^{oe}) + E^{\text{LL}}(f^{oo})| \\
&\leq |E^{\text{MM}}(f^{ee})| + |E^{\text{ML}}(f^{eo})| + |E^{\text{LM}}(f^{oe})| + |E^{\text{LL}}(f^{oo})| \\
&\lesssim \frac{1}{L^{m+4}}.
\end{aligned} \quad (3.44)$$

Therefore, the proof is completed by combining (3.34), (3.35) and (3.44). \square

For the FS-MM method, our goal is to estimate the error $\|\varphi - \varphi_N\|_{\infty(\Omega)}$, where $\varphi = U * \rho$ and φ_N is given by (2.23). In fact, the error primarily comes from the discretization of the Fourier integral via the midpoint quadrature. We present the following theorem for its rigorous analysis.

Theorem 3 (FS-MM method). *For a smooth and compactly supported function $\rho(\mathbf{x})$ that satisfies the vanishing moment condition (1.3), the following estimate*

$$\|\varphi - \varphi_N\|_{\infty(\Omega)} \lesssim \sum_{|\beta|=m+1} \max_{\substack{\mathbf{x} \in \partial\Omega \\ \mathbf{y} \in \Omega_0 \\ 0 \leq s \leq 1}} |\partial^\beta U(\mathbf{x} - s\mathbf{y})|$$

holds true where $\Omega_0 := \text{supp}\{\rho\} \subset \Omega$.

Proof. Since $\hat{\rho}$ is compactly supported, it is reasonable to choose a fixed h such that $\text{supp}\{\hat{\rho}\} \subsetneq R_h := [-\pi/h, \pi/h]^d$. Therefore, the error comes from the discretization of the integral using the midpoint quadrature, i.e.,

$$\varphi - \varphi_N = I(f) - Q_N^M(f) = E_N^M(f),$$

where $f(\mathbf{k}) = \hat{U}(\mathbf{k})\hat{\rho}(\mathbf{k})e^{i\mathbf{k}\cdot\mathbf{x}}$, $I(f)$ represents the integral of the function f over R_h , $Q_N^M(f)$ denotes the midpoint quadrature with N points in each direction and $E_N^M(f)$ represents the corresponding error.

Similar to the proof in Theorem 2, by taking the 2D case as an example, we can obtain

$$\begin{aligned} |E_{NN}^{MM}(f^{ee})| &\lesssim \max_{\substack{\mathbf{x} \in \partial\Omega \\ \mathbf{y} \in \Omega_0 \\ 0 \leq s \leq 1}} |\partial^\beta U(\mathbf{x} - s\mathbf{y})|, \quad |E_{NN}^{ML}(f^{eo})| \lesssim \max_{\substack{\mathbf{x} \in \partial\Omega \\ \mathbf{y} \in \Omega_0 \\ 0 \leq s \leq 1}} |\partial^\beta U(\mathbf{x} - s\mathbf{y})|, \\ |E_{NN}^{LM}(f^{oe})| &\lesssim \max_{\substack{\mathbf{x} \in \partial\Omega \\ \mathbf{y} \in \Omega_0 \\ 0 \leq s \leq 1}} |\partial^\beta U(\mathbf{x} - s\mathbf{y})|, \quad |E_{NN}^{LL}(f^{oo})| \lesssim \max_{\substack{\mathbf{x} \in \partial\Omega \\ \mathbf{y} \in \Omega_0 \\ 0 \leq s \leq 1}} |\partial^\beta U(\mathbf{x} - s\mathbf{y})|. \end{aligned}$$

With the help of the relation between midpoint rule and left rectangle rule, i.e.,

$$Q_{NN}^{MM}(f) + Q_{NN}^{ML}(f) = 2Q_{N(2N)}^{ML}(f),$$

we have

$$\begin{aligned} E_{NN}^{MM}(f) &= I(f) - Q_{NN}^{MM}(f) = I(f) - \left[2Q_{N(2N)}^{ML}(f) - Q_{NN}^{ML}(f) \right] \\ &= 2\left[I(f) - Q_{N(2N)}^{ML}(f) \right] - \left[I(f) - Q_{NN}^{ML}(f) \right] \\ &= 2E_{N(2N)}^{ML}(f) - E_{NN}^{ML}(f). \end{aligned}$$

In a similar way, we obtain

$$E_{NN}^{MM}(f) = 2E_{(2N)N}^{LM}(f) - E_{NN}^{LM}(f), \quad E_{NN}^{ML}(f) = 2E_{(2N)N}^{LL}(f) - E_{NN}^{LL}(f).$$

Therefore, we have

$$\begin{aligned} |\varphi - \varphi_N| = |E_{NN}^{MM}(f)| &\leq |E_{NN}^{MM}(f^{ee})| + |E_{NN}^{MM}(f^{eo})| + |E_{NN}^{MM}(f^{oe})| + |E_{NN}^{MM}(f^{oo})| \\ &\lesssim |E_{NN}^{MM}(f^{ee})| + |E_{NN}^{ML}(f^{eo})| + |E_{NN}^{LM}(f^{oe})| + |E_{NN}^{LL}(f^{oo})| \\ &\lesssim \sum_{|\beta|=m+1} \max_{\substack{\mathbf{x} \in \partial\Omega \\ \mathbf{y} \in \Omega_0 \\ 0 \leq s \leq 1}} |\partial^\beta U(\mathbf{x} - s\mathbf{y})|. \end{aligned}$$

Then the proof is completed. \square

4. Numerical results

In this section, we shall investigate the accuracy and efficiency for different nonlocal potentials in both 2D and 3D cases. The computational domain \mathbf{R}_L is discretized uniformly in each spatial direction with mesh size h_j , and we define mesh size vector as $\mathbf{h} = (h_1, \dots, h_d)$. For simplicity, we shall use h to denote the mesh size if all the mesh sizes are equal. All numerical errors are calculated in the relative maximum

norm, defined as follows

$$\mathcal{E} := \max_{\mathbf{x} \in \mathcal{T}_h} |\varphi(\mathbf{x}) - \varphi_h(\mathbf{x})| / \max_{\mathbf{x} \in \mathcal{T}_h} |\varphi(\mathbf{x})|,$$

where φ_h is the numerical solution on mesh grid \mathcal{T}_h and φ is the reference solution.

Unless otherwise specified, we use the auxiliary function (1.7) with $\sigma = 2$ and the density functions $\rho(\mathbf{x}) = e^{-|\mathbf{x}-\mathbf{x}_0|^2/4}$, where $\mathbf{x}_0 = (1, 2)$ for $d = 2$ and $\mathbf{x}_0 = (1, 2, 3)$ for $d = 3$. The solution obtained by KTM [20] is taken as the reference solution. In practice, we choose computational domain $\mathbf{R}_L = [-16, 16]^d$ and mesh size $h = 1/4$.

4.1. The Poisson potentials in 2D/3D

Example 1 (Accuracy test). Here, we consider the 2D and 3D Poisson potentials with convolution kernel

$$U(\mathbf{x}) = \begin{cases} -\frac{1}{2\pi} \ln(|\mathbf{x}|), & d = 2, \\ \frac{1}{4\pi|\mathbf{x}|}, & d = 3. \end{cases}$$

Figure 1 shows the errors and convergence orders with respect to the domain expansion factor S . From these results, we can see that the convergence order is at least $m + 1$ for the 2D Poisson potential and $m + 2$ for the 3D Poisson potential. It is compatible with theoretical error estimates and performs better for certain m .

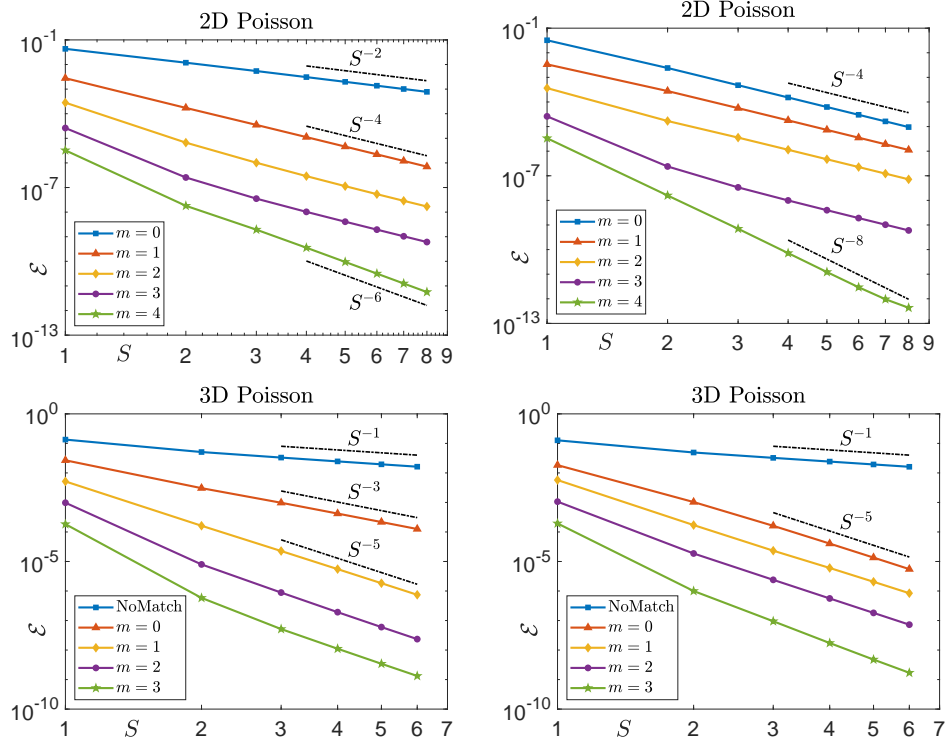


Figure 1: Errors of the SP-MM (left) and FS-MM (right) methods for Poisson potentials.

Example 2 (Efficiency test). To investigate the efficiency, we present the performance of SP-MM and FS-MM methods with/without tensor acceleration in terms of CPU time, where we choose the 3D Poisson potentials with $m = 2$. The computation of tensor version is split into two parts: the precomputation part

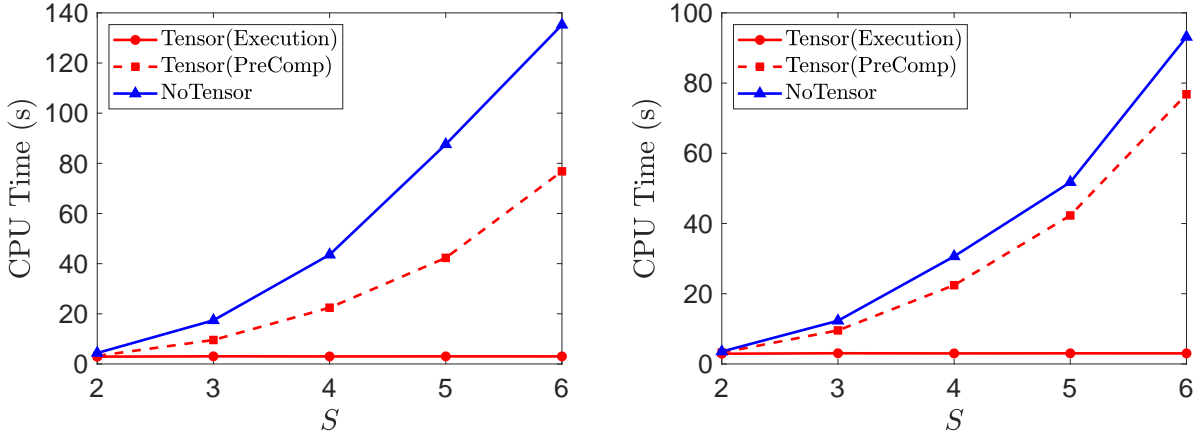


Figure 2: Timing results of SP-MM (left) and FS-MM (right) methods, with/without tensor acceleration, versus domain expansion factor S .

(**PreComp**) and the execution part (**Execution**). The algorithms were implemented in Matlab (2016a) and run on a 3.00GHz Intel(R) Xeon(R) Gold 6248R CPU with a 36 MB cache in Ubuntu GNU/Linux.

In Figure 2, we present the CPU time for different domain expansion factor S . We can conclude that, for tensor version, once the precomputation step is done, the effective computation involves only a pair of FFT/iFFT on vectors of twice the length in each direction, regardless of the magnitude of domain expansion factor S . This is of significant importance in practical simulation, especially when the potential evaluation needs to be performed multiple times under the same setups.

4.2. The 2D Coulomb potentials and 3D DDI

Example 3. Here, we consider the following potentials

- **2D Coulomb potential:** The kernel is given as $U(\mathbf{x}) = \frac{1}{2\pi|\mathbf{x}|}$.

- **3D DDI:** The kernel is given as

$$U(\mathbf{x}) = \frac{3}{4\pi} \frac{\mathbf{m} \cdot \mathbf{n} - 3(\mathbf{x} \cdot \mathbf{m})(\mathbf{x} \cdot \mathbf{n})/|\mathbf{x}|^2}{|\mathbf{x}|^3},$$

where $\mathbf{n}, \mathbf{m} \in \mathbb{R}^3$ are unit vectors representing the dipole orientations, and the 3D potential is reformulated as [4]:

$$\varphi(\mathbf{x}) = -(\mathbf{m} \cdot \mathbf{n})\rho(\mathbf{x}) - 3\frac{1}{4\pi|\mathbf{x}|} * (\partial_{\mathbf{nm}}\rho),$$

where $\partial_{\mathbf{m}} = \mathbf{m} \cdot \nabla$ and $\partial_{\mathbf{nm}} = \partial_{\mathbf{n}}(\partial_{\mathbf{m}})$. In fact, the potential can be calculated via the 3D Poisson potential with source term $\partial_{\mathbf{nm}}\rho$, which can be easily computed numerically via Fourier spectral method.

Figure 3 presents the errors and convergence orders with respect to the domain expansion factor S . The results indicate that the convergence order is at least $m + 2$, i.e., $\mathcal{O}(S^{-(m+2)})$, for both 2D Coulomb potential and 3D DDI. For the 3D DDI, results obtained by SP method and SP-MM method with $m = 0, 1$ are identical to each other, and it is because moments of $\partial_{\mathbf{nm}}\rho$ vanish up to order 1 automatically.

To demonstrate the numerical performance of the proposed methods, we compare them with the well-established KTM and ATKM methods in terms of implementation, accuracy and efficiency. Among these methods, our methods are the easiest to implement. Figure 4 presents log-log plots of computational time

versus errors for the 2D Coulomb potential with density $\rho = e^{-4(x^2+y^2)}$. From these results, we observe that when the accuracy requirement is not very high (e.g., $\geq 10^{-11}$), our methods are more efficient.

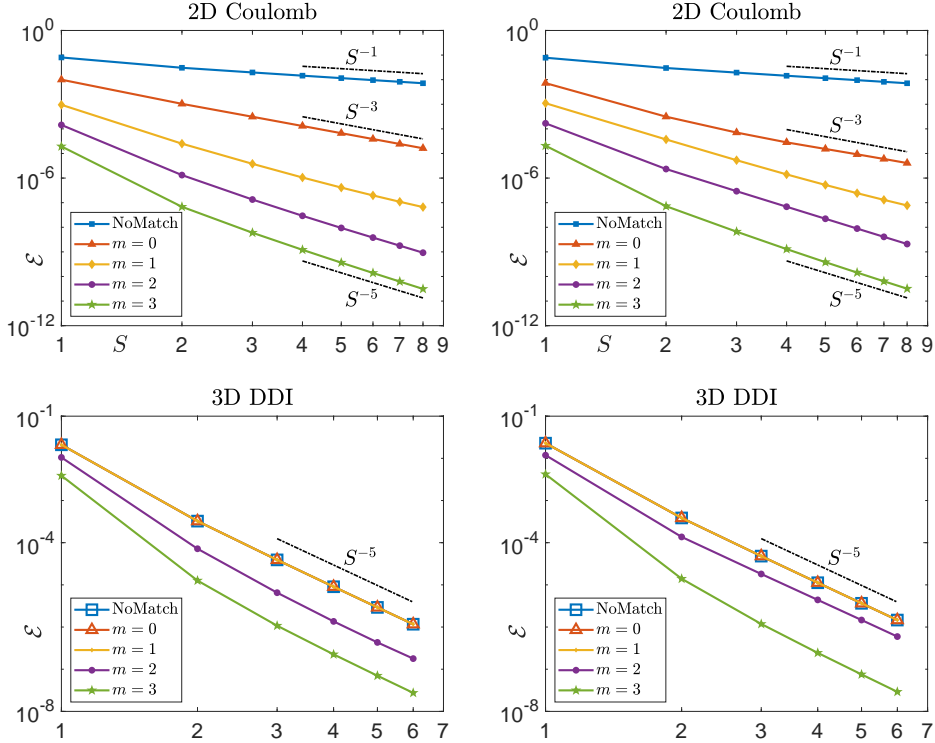


Figure 3: Errors of SP-MM (left) and FS-MM (right) methods for Coulomb potentials and DDI.

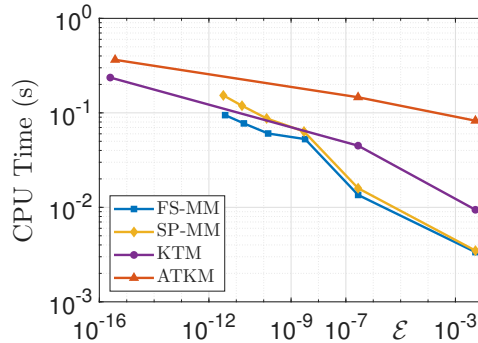


Figure 4: Log-log plots of timing results versus errors for Coulomb potential in Example 3.

4.3. The Biharmonic potentials in 2D/3D

Example 4. Here, we consider the 2D and 3D Biharmonic potentials with convolution kernel

$$U(\mathbf{x}) = \begin{cases} -\frac{1}{8\pi}|\mathbf{x}|^2(\ln(|\mathbf{x}|) - 1), & d = 2, \\ \frac{1}{8\pi}|\mathbf{x}|, & d = 3. \end{cases}$$

Figure 5 shows the errors and convergence orders with respect to the domain expansion factor S . From these results, we can see that the convergence order is at least $m - 1$ for the 2D Biharmonic potential and m for the 3D Biharmonic potential, which is consistent with the theoretical results.

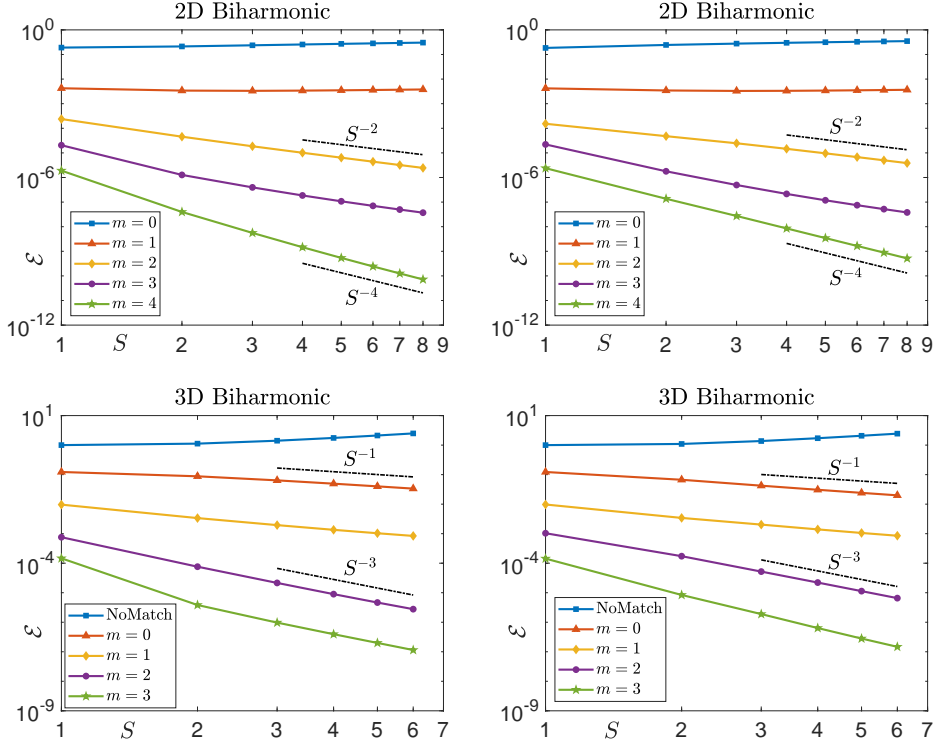


Figure 5: Errors of the SP-MM (left) and SP-Tensor (right) methods for Biharmonic potentials.

4.4. The Yukawa potentials in 2D/3D

Example 5. Here, we consider the 2D and 3D Yukawa potentials with convolution kernel

$$U(\mathbf{x}) = \begin{cases} \frac{1}{2\pi} K_0(\lambda|\mathbf{x}|), & d = 2, \\ \frac{1}{4\pi|\mathbf{x}|} e^{-\lambda|\mathbf{x}|}, & d = 3, \end{cases}$$

where $K_0(r)$ is modified Bessel functions of the second kind with order 0 [1]. For a Gaussian density $\rho(\mathbf{x}) = e^{-|\mathbf{x}|^2/\sigma^2}$, the Yukawa potentials are given explicitly as [11]

$$\varphi(\mathbf{x}) = \begin{cases} \int_0^\infty K_0(\lambda s) s e^{-\frac{r^2+s^2}{\sigma^2}} I_0\left(\frac{2rs}{\sigma^2}\right) ds, & d = 2, \\ (\sqrt{\pi}\sigma)^3 \frac{e^{-\lambda r + \frac{\lambda^2\sigma^2}{4}}}{8\pi r} [\operatorname{erfc}\left(-\frac{r}{\sigma} + \frac{\lambda\sigma}{2}\right) - e^{2\lambda r} \operatorname{erfc}\left(\frac{r}{\sigma} + \frac{\lambda\sigma}{2}\right)], & d = 3, \end{cases}$$

where $I_0(r)$ is the modified Bessel function of order zero and $\operatorname{erfc}(r) = 1 - \frac{2}{\sqrt{\pi}} \int_0^r e^{-t^2} dt$ is the complementary error function [1].

Note that the kernel $K_0(\lambda r)$ and $e^{-\lambda r}/r$ decay exponentially to zero at infinity and the decay rate grows as $|\lambda|$ gets larger. This property makes the SP method highly effective. Table 2 presents the errors with different λ and S . The results demonstrate that, with the help of the expanding domain technique, this method can readily achieve high accuracy.

Table 2: Errors of 2D/3D Yukawa potentials in Example 5.

		$S = 1$	$S = 2$	$S = 3$
2D	$\lambda = 1$	1.9058E-07	3.7234E-16	3.7234E-16
	$\lambda = 2$	5.3590E-13	3.5729E-16	4.0353E-16
	$\lambda = 3$	4.2084E-16	3.6387E-16	4.1278E-16
3D	$\lambda = 1$	8.2316E-08	4.0121E-16	6.8779E-16
	$\lambda = 2$	2.8871E-13	3.5191E-15	3.5191E-15
	$\lambda = 3$	6.3361E-15	6.3361E-15	6.6241E-15

5. Conclusions

We proposed two simple and accurate fast algorithms to compute the convolution potential based on moment-matching for the density. Each method requires merely minor modifications to popular sine pseudospectral (SP)/Fourier spectral (FS) method and achieves arbitrary high order convergence. To this end, we split the potential into two part, i.e., $\varphi = U * \rho_1 + U * (\rho - \rho_1) := \varphi_1 + \varphi_2$, where the moments of auxiliary function ρ_1 match those of ρ up to order m . The auxiliary function ρ_1 is constructed as a linear combination of Gaussian and its derivatives, and potential φ_1 can be computed analytically or integrated numerically with ease. For the smooth residual density $\rho_2 = \rho - \rho_1$, its moments vanish up to order m and the Fourier transform $\hat{\rho}_2(\mathbf{k})$ decays exponentially fast at the far field.

In the first method, one solves a differential/pseudo-differential equation with homogeneous Dirichlet boundary conditions using SP. While, in the second method, we discretize the Fourier integral by trapezoidal/midpoint rule. Rigorous error estimates were provided to confirm the $\mathcal{O}(L^{-p})$ convergence on domain $\Omega = [-L, L]^d$ for both methods, where the integer p depends on order m and the kernel U . To further improve the numerical accuracy and efficiency, we employ the domain expansion technique and simplify each resulting quadrature into one discrete convolution. The execution finally boils down to discrete Fast Fourier transform on a double-sized vector, which is of essential importance for long-time simulation in terms of efficiency, especially when the potential is evaluated multiple times under the same setups.

Acknowledgements

This work was partially supported by the National Key R&D Program of China (No. 2024YFA1012803), the National Natural Science Foundation of China (No. 11971335) and the Institutional Research Fund from Sichuan University (No. 2020SCUNL110) (Q. Tang), and the National Natural Science Foundation of China (No.12271400) and Tianyuan Mathematical center in Southwest China (No. 12226102) (X. Liu and Y. Zhang).

Appendix A. Coefficients γ_α

Specifically, the coefficients γ_α are determined by the linear system (2.15). For the sake of simplicity, we define $H_\beta^\alpha := \int_{\mathbb{R}^d} \frac{\partial^\alpha G(\mathbf{x})}{\partial \mathbf{x}^\alpha} \mathbf{x}^\beta d\mathbf{x}$ and $P_\beta := \int_{\mathbb{R}^d} \rho(\mathbf{x}) \mathbf{x}^\beta d\mathbf{x}$, then, the linear system (2.15) can be rewritten as

$$\sum_{|\alpha|=0}^m H_\beta^\alpha \gamma_\alpha = P_\beta, \quad |\beta| = 0, \dots, m. \quad (\text{A.1})$$

Here, H_β^α can be evaluated analytically and P_β can be well approximated using the trapezoidal quadrature. Given a fixed m , we need to compute $\frac{(m+d)!}{m!d!}$ coefficients for $d = 1, 2, 3$. Here, we claim that matrix H_β^α is lower triangular if the auxiliary function $G(\mathbf{x})$ is symmetric and compactly supported. This observation suggests the solution to (A.1) can be obtained by back substitution. Table ?? and Table ?? list the explicit

formulas for coefficients γ_{α} . Taking the 2D case as an example, the matrix H_{β}^{α} has the following properties.

Proposition 1. Denote the coefficient matrix by

$$H_{(\beta_1, \beta_2)}^{(\alpha_1, \alpha_2)} = \int_{\mathbb{R}^2} \frac{\partial^{(\alpha_1 + \alpha_2)} G(\mathbf{x})}{\partial x_1^{\alpha_1} x_2^{\alpha_2}} x_1^{\beta_1} x_2^{\beta_2} dx_1 dx_2.$$

If the function $G(\mathbf{x})$ is symmetric and compactly supported, the following properties

- (i) If $\alpha_i + \beta_i$ is odd for some i , then $H_{(\beta_1, \beta_2)}^{(\alpha_1, \alpha_2)} = 0$,
- (ii) Symmetry: $H_{(\beta_1, \beta_2)}^{(\alpha_1, \alpha_2)} = H_{(\beta_2, \beta_1)}^{(\alpha_2, \alpha_1)}$,
- (iii) Recurrence formula: $H_{(\beta_1, \beta_2)}^{(\alpha_1, \alpha_2)} = -\beta_1 H_{(\beta_1-1, \beta_2)}^{(\alpha_1-1, \alpha_2)}$,
- (iv) If $\alpha_i > \beta_i$ for some i , then $H_{(\beta_1, \beta_2)}^{(\alpha_1, \alpha_2)} = 0$,

hold true.

Proof. It is straightforward to verify that properties (i) and (ii) hold. For property (iii), using integration by parts, we have

$$\begin{aligned} H_{(\beta_1, \beta_2)}^{(\alpha_1, \alpha_2)} &= \int_{-\infty}^{\infty} \left[\int_{-\infty}^{\infty} \frac{\partial^{(\alpha_1 + \alpha_2)} G(\mathbf{x})}{\partial x_1^{\alpha_1} x_2^{\alpha_2}} x_1^{\beta_1} dx_1 \right] x_2^{\beta_2} dx_2 \\ &= \int_{-\infty}^{\infty} \left[-\beta_1 \int_{-\infty}^{\infty} \frac{\partial^{(\alpha_1 + \alpha_2 - 1)} G(\mathbf{x})}{\partial x_1^{\alpha_1-1} x_2^{\alpha_2}} x_1^{\beta_1-1} dx_1 \right] x_2^{\beta_2} dx_2 = -\beta_1 H_{(\beta_1-1, \beta_2)}^{(\alpha_1-1, \alpha_2)}. \end{aligned}$$

For property (iv), due to the fact that function $G(\mathbf{x})$ is compactly supported, we have the following assertion:

$$\text{If } \alpha_i \neq 0, \beta_i = 0 \text{ for some } i, \text{ then } H_{(\beta_1, \beta_2)}^{(\alpha_1, \alpha_2)} = 0. \quad (\text{A.2})$$

Without loss of generality, we assume that $\alpha_1 \neq 0, \beta_1 = 0$, then

$$H_{(\beta_1, \beta_2)}^{(\alpha_1, \alpha_2)} = \int_{-\infty}^{\infty} \left[\int_{-\infty}^{\infty} \frac{\partial^{(\alpha_1 + \alpha_2)} G(\mathbf{x})}{\partial x_1^{\alpha_1} x_2^{\alpha_2}} dx_1 \right] x_2^{\beta_2} dx_2 = 0.$$

Combining property (iii) and (A.2), we see that if $\alpha_1 > \beta_1$,

$$H_{(\beta_1, \beta_2)}^{(\alpha_1, \alpha_2)} = (-1)^{\beta_1} \beta_1! H_{(0, \beta_2)}^{(\alpha_1 - \beta_1, \alpha_2)} = 0.$$

Obviously, using the symmetry property (ii), we have $H_{(\beta_1, \beta_2)}^{(\alpha_1, \alpha_2)} = 0$ if $\alpha_2 > \beta_2$. \square

Theorem 4. The matrix $H_{\beta}^{\alpha} = \int_{\mathbb{R}^2} \frac{\partial^{(\alpha_1 + \alpha_2)} G(\mathbf{x})}{\partial x_1^{\alpha_1} x_2^{\alpha_2}} x_1^{\beta_1} x_2^{\beta_2} dx_1 dx_2$ is lower triangular if function $G(\mathbf{x})$ is symmetric and compactly supported.

Proof. It is sufficient to show that $H_{(\beta_1, \beta_2)}^{(\alpha_1, \alpha_2)} = 0$ if $\alpha_1 + \alpha_2 \geq \beta_1 + \beta_2$ and $(\alpha_1, \beta_1) \neq (\alpha_2, \beta_2)$, which can be proved by (iv) in Proposition 1. To be specific, if $\alpha_1 > \beta_1$, it follows from (iv) that $H_{(\beta_1, \beta_2)}^{(\alpha_1, \alpha_2)} = 0$. Otherwise, if $\alpha_1 \leq \beta_1$, which means that $\alpha_2 > \beta_2$, then $H_{(\beta_1, \beta_2)}^{(\alpha_1, \alpha_2)} = 0$ by (iv). \square

Table A1: Coefficients γ_α with $|\alpha| = 0, 1, 2, 3, 4$ for the 2D case.

$\gamma_{00} = P_{00}$			
$\gamma_{01} = -P_{01}$	$\gamma_{10} = -P_{10}$		
$\gamma_{02} = \frac{1}{2}(P_{02} - \sigma^2 \gamma_{00})$	$\gamma_{11} = P_{11}$	$\gamma_{20} = \frac{1}{2}(P_{20} - \sigma^2 \gamma_{00})$	
$\gamma_{03} = \frac{1}{6}(-P_{03} - 3\sigma^2 \gamma_{01})$	$\gamma_{12} = \frac{1}{2}(-P_{12} - \sigma^2 \gamma_{10})$	$\gamma_{21} = \frac{1}{2}(-P_{21} - \sigma^2 \gamma_{01})$	$\gamma_{30} = \frac{1}{6}(-P_{30} - 3\sigma^2 \gamma_{10})$
$\gamma_{04} = \frac{1}{24}(P_{04} - 3\sigma^4 \gamma_{00} - 12\sigma^2 \gamma_{02})$	$\gamma_{13} = \frac{1}{6}(P_{13} - 3\sigma^2 \gamma_{11})$	$\gamma_{22} = \frac{1}{4}(P_{22} - \sigma^4 \gamma_{00} - 2\sigma^2 \gamma_{20} - 2\sigma^2 \gamma_{02})$	$\gamma_{31} = \frac{1}{6}(P_{31} - 3\sigma^2 \gamma_{11})$
$\gamma_{40} = \frac{1}{24}(P_{40} - 3\sigma^4 \gamma_{00} - 12\sigma^2 \gamma_{20})$			

Table A2: Coefficients γ_α with $|\alpha| = 0, 1, 2, 3$ for the 3D case..

$\gamma_{000} = P_{000}$			
$\gamma_{001} = -P_{001}$	$\gamma_{010} = -P_{010}$	$\gamma_{100} = -P_{100}$	
$\gamma_{002} = \frac{1}{2}(P_{002} - \sigma^2 \gamma_{000})$	$\gamma_{011} = P_{011}$	$\gamma_{020} = \frac{1}{2}(P_{020} - \sigma^2 \gamma_{000})$	$\gamma_{101} = P_{101}$
$\gamma_{110} = P_{110}$	$\gamma_{200} = \frac{1}{2}(P_{200} - \sigma^2 \gamma_{000})$		
$\gamma_{003} = \frac{1}{6}(-P_{003} - 3\sigma^2 \gamma_{001})$	$\gamma_{012} = \frac{1}{2}(-P_{012} - \sigma^2 \gamma_{010})$	$\gamma_{021} = \frac{1}{2}(-P_{021} - \sigma^2 \gamma_{001})$	$\gamma_{030} = \frac{1}{6}(-P_{030} - 3\sigma^2 \gamma_{010})$
$\gamma_{102} = \frac{1}{2}(-P_{102} - \sigma^2 \gamma_{100})$	$\gamma_{111} = -P_{111}$	$\gamma_{120} = \frac{1}{2}(-P_{120} - \sigma^2 \gamma_{100})$	$\gamma_{201} = \frac{1}{2}(-P_{201} - \sigma^2 \gamma_{001})$
$\gamma_{210} = \frac{1}{2}(-P_{210} - \sigma^2 \gamma_{010})$	$\gamma_{300} = \frac{1}{6}(-P_{300} - 3\sigma^2 \gamma_{100})$		

Appendix B. Analytical expression $W(\mathbf{x})$

- The d-dimensional Poisson potential.

$$W(\mathbf{x}) = \begin{cases} -\frac{1}{4\pi} \left[E_1 \left(\frac{r^2}{2\sigma^2} \right) + 2 \ln(r) \right], & d = 2, \\ \frac{1}{4\pi|\mathbf{x}|} \operatorname{Erf} \left(\frac{r}{\sqrt{2}\sigma} \right), & d = 3. \end{cases}$$

Here, $E_1(r) = \int_r^\infty t^{-1} e^{-t} dt$ is the exponential integral function and $\operatorname{Erf}(r) = \frac{2}{\sqrt{\pi}} \int_0^r e^{-t^2} dt$ is the error function [1, 11].

- The 2D Coulomb potential.

$$W(\mathbf{x}) = \frac{1}{2\sqrt{2\pi}\sigma} I_0 \left(\frac{r^2}{4\sigma^2} \right) e^{-\frac{r^2}{4\sigma^2}},$$

where $I_0(r)$ is the modified Bessel function of order zero [1, 11].

- The d-dimensional Biharmonic potential.

$$W(\mathbf{x}) = \begin{cases} \frac{1}{8\pi} \left[r^2 + e^{-\frac{r^2}{\sigma^2}} \sigma^2 \right] + \frac{1}{16} (r^2 + 2\sigma^2) \left[\operatorname{Ei} \left(-\frac{r^2}{2\sigma^2} \right) - 2 \ln(r) \right], & d = 2, \\ \frac{1}{8\pi} \left[\operatorname{Erf} \left(\frac{r}{\sqrt{2}\sigma} \right) \left(\frac{\sigma^2}{r} + r \right) + \sigma \sqrt{\frac{2}{\pi}} e^{-\frac{r^2}{2\sigma^2}} \right], & d = 3. \end{cases}$$

Here, $\operatorname{Ei}(r) := \int_{-\infty}^r t^{-1} e^t dt$ is the exponential integral [1, 11].

References

- [1] M. ABRAMOWITZ AND I. A. STEGUN, *Handbook of mathematical functions*, Dover, 1965.
- [2] C. R. ANDERSON, *A recursive expanding domain method for the solution of Laplace's equation in infinite domains*, Technical report CAM-14-45, Department of Mathematics, UCLA, Los Angeles, California, 2014.
- [3] C. R. ANDERSON, *High order expanding domain methods for the solution of Poisson's equation in infinite domains*, J. Comput. Phys., **314** (2016), 194-205.
- [4] W. BAO AND Y. CAI, *Mathematical theory and numerical methods for Bose-Einstein condensation*, Kinet. Relat. Models, **6** (2013), 1-135.
- [5] W. BAO, Y. CAI AND H. WANG, *Efficient numerical methods for computing ground states and dynamics of dipolar Bose-Einstein condensates*, J. Comput. Phys., **229** (2010), 7874-7892.
- [6] W. BAO, H. JIAN, N. MAUSER AND Y. ZHANG, *Dimension reduction of the Schrödinger equation with Coulomb and anisotropic confining potentials*, SIAM J. Appl. Math., **73** (2013), 2100-2123.
- [7] W. BAO, N. MAUSER AND H. P. STIMMING, *Effective one particle quantum dynamics of electrons: A numerical study of the Schrödinger-Poisson-Xα model*, Comm. Math. Sci., **1** (2003), 809-831.
- [8] W. BAO, S. JIANG, Q. TANG AND Y. ZHANG, *Computing the ground state and dynamics of the nonlinear Schrödinger equation with nonlocal interactions via the nonuniform FFT*, J. Comput. Phys., **296** (2015), 72-89.
- [9] L. EXL, N. MAUSER AND Y. ZHANG, *Accurate and efficient computation of nonlocal potentials based on Gaussian-sum approximation*, J. Comput. Phys., **327** (2016), 629-642.
- [10] L. GREENGARD, S. JIANG M. RACHH AND J. WANG, *A new version of the adaptive fast Gauss transform for discrete and continuous sources*, SIAM Review, **66** (2024), 287-315.
- [11] L. GREENGARD, S. JIANG AND Y. ZHANG, *The anisotropic truncated kernel method for convolution with free-space Green's functions*, SIAM J. Sci. Comput., **38** (2018), A3733-A3754.
- [12] S. JIANG, L. GREENGARD AND W. BAO, *Fast and accurate evaluation of nonlocal Coulomb and dipole-dipole interactions via the nonuniform FFT*, SIAM J. Sci. Comput., **36** (2014), 777-794.
- [13] T. LAHAYE, C. MENOTTI, L. SANTOS, M. LEWENSTEIN AND T. PFAU, *The physics of dipolar bosonic quantum gases*, Rep. Prog. Phys., **72** (2009), arctile 126401.
- [14] X. LIU, Q. TANG, S. ZHANG AND Y. ZHANG, *On optimal zero-padding of kernel truncation method*, SIAM J. Sci. Comput., **46** (2024), A23-A49.
- [15] X. LIU AND Y. ZHANG, *Fast convolution solver based on far-field smooth approximation*, J. Comput. Phys., **554** (2026), article 114753.
- [16] N. MAUSER AND Y. ZHANG, *Exact artificial boundary condition for the Poisson equation in the simulation of the 2D Schrödinger-Poisson system*, Commun. Comput. Phys., **16** (2014), 764-780.
- [17] C. A. ROZZI, D. VARSANO, A. MARINI, E. K. U. GROSS AND A. RUBIO, *Exact Coulomb cutoff technique for supercell calculations*, Phys. Rev. B, **73** (2006), article 205119.
- [18] J. SHEN, T. TANG AND L. WANG, *Spectral Methods: Algorithms, Analysis and Applications*, Springer, 2011.
- [19] M. H. PROTTER AND H. F. WEINBERGER, *Maximum principles in differential equations*, Springer Science & Business Media, 2012.
- [20] F. VICO, L. GREENGARD AND M. FERRANDO, *Fast convolution with free-space Green's functions*, J. Comput. Phys., **323** (2016), 191-203.
- [21] S. YI AND L. YOU, *Trapped condensates of atoms with dipole interactions*, Phys. Rev. A, **63** (2001), article 053607.